Advanced long period fiber grating and its applications to fiber sensor and optical filter

静岡大学博士論文

Advanced long period fiber grating and its applications to fiber sensor and optical filter
長周期ファイバグレーティング及びそのファイバセンサー・光フィルターへの応用

王　鵬

大学院自然科学系教育部

光・ナノ物質機能専攻

2016 年 12 月

Abstract

With the development of the fiber optics, fiber gratings have already played a very important role in the field of optical communication and optical sensor systems. There are two kinds of fiber grating: fiber Bragg gratings (FBGs) and long period fiber gratings (LPGs). Compared with FBGs' practical applications in the industry, the applications of LPGs are not intensively developed. Attributed to the copropagating mode coupling mechanism, LPG can be utilized as a gain flattening filter or a chromatic dispersion compensation. Moreover, since the cladding mode is largely sensitive to the surrounding refractive index, LPG is also an excellent candidate for a fiber-type refractive-index sensor.

In this thesis, we have concentrated our research works on the optimal design and fabrication of the LPG, especially for the helical type LPGs, and explore its potential applications to the fields of fiber sensor and optical communication.

Firstly, a brief overview was given about the basic techniques for fiber gratings, including the classification, fabrication and application of long period fiber gratings especially in sensing fields. The characteristics of LPG were theoretically investigated based on the coupled mode theory and the transfer matrix method.

Secondly, we have proposed and demonstrated a new method for writing phase-shifted LPGs which is based on the utilization of the CO_2 laser technique. By using the proposed method, several kinds of phase-shifted LPGs were fabricated and experimentally investigated, where both the grating and the inserted phase-shift were obtained simultaneously. As a particularly example of this kind of LPGs, a robust temperature-insensitive sensor that allows for large strain measurement up to 7600 $\mu\varepsilon$ was proposed and successfully demonstrated, which is based the on the utilization of a

π phase-shifted LPG.

Thirdly, we have proposed a new kind of LPGs with a helical structure (HLPG). We have developed a general coupled-mode theory for this kind gratings. A new fabrication method of the HLPGs by using CO_2 laser technique has been proposed and experimentally demonstrated, where a sapphire tube is particularly utilized in place of the generally used focal-lens, this is the firstly report to fabricate the thinned HLPGs with this technique. The proposed method allows to fabricate the HLPGs with a diameter less than several tens of micrometer. In order to compare with the experimental results, some of the theoretical simulations have also been done, which are related to changes of the resonant wavelengths of HLPGs under the condition of three different fiber diameters. As an application of this kind of HLPGs, a novel HLPGs-based refractometric sensor that allows for temperature-free measurement of the refractive index is proposed and experimentally demonstrated.

Finally, we have been trying to explore some applications of HLPG in the field of fiber optics, especially for the fiber-based optical filter. We have proposed and demonstrated a novel method for the fabrication of flat-top band-rejection, which is realized by successively cascading two HLPGs but with opposite helicities. The proposed HLPGs have a relative short length (less than 4.6 cm) and do not require a complex apodization in grating's amplitude, which makes this kind of HLPGs particularly suitable being fabricated by using the robust CO_2 laser writing technique.

Keyword: Optical communication, optical sensor, long period fiber grating, fiber Bragg grating, helical long-period fiber grating, cascaded long-period fiber grating, flat-top band rejection filter

Acknowledgements

I would like to express my thanks to:

- *My supervisor, Prof. Hongpu Li, for his constant encouragement, guidance and support through-out my research project. Prof. Li, a respectable, responsible and resourceful scholar, who has provided me with valuable guidance in every stage of the research life. He provided me such a good opportunity to study in his laboratory and guided me into an important field of fiber sensor and fiber optical communication. Prof. Li shared his valuable knowledge and experience not only on my study but also on my Japanese life. The most important, I will heartily grateful to him for his generous, confidence and care on my research. Because of the presence of Prof. Li, my Japanese study life is the most exciting.*
- *Prof. Norihisa Hiromoto, Prof. Hirokazu Tatsuoka, and Prof. Atsushi Nakamura, who carefully review my thesis and give me a lot of invaluable comments.*
- *Prof. Zhao, who provides me a lot of help while I am writing my doctor thesis.*
- *Dr. Lunlun Xian, Mr. Ramanathan Subramanian and Mr. Chengliang Zhu, who share their knowledge and experiences to me in my research life. Also they gave me a lot of suggestions both in my research and my daily life in Japan.*
- *The students in Li`s lab, Jiexin Song, Kajiyama Yuki, Shuichiro*

Kanada, Shoma Ishigami, Suzuki for constructive discussions and debates and providing a positive academic atmosphere in the laboratory and help me to adapt to the daily life in Japan.

- *My beloved parents and beloved wife as well as the other members in my family, for their love, unselfish supports and understanding for my studying aboard.*
- *Other friends, for their great help and supports in my Japanese life.*

Contents

1. Introduction

1.1 Research background

In the past 40 years, optical fiber has been widely used in the fields such as optical communication, optical sensing, nonlinear optics and optical power transmission etc. In 2009, Charles K. Kao was jointly awarded the Nobel Prize in Physics for “Groundbreaking achievements concerning the transmission of light in fibers for optical communication”. In long-haul communication system, the propagation losses for the current single-mode fiber have been reduced to ～0.2dB/km. As a matter of fact, up to now the total length of the global laying of the cable can be combined around the earth more than 30 laps of the equator.

Optical fiber sensor which is accompanied by optical fiber and optical fiber communication technology is a new sensing technology, which began to develop in the middle of the last century, combined with the development of optical communication technology, laser technology and sensor technology. Sensors are devices that perform information acquisition, transmission and conversion. In general, the sensors can transform a signal from a sensing element to another form. So it is true multidisciplinary technology, such as electronics, mechanics, chemistry, and so on. The optical fiber sensor is based on the utilization of either the fiber or the fiber-based devices as a functional material in order to complete the measurement from non-optical conversion. Optical fiber sensor uses light as the information carrier, and makes use of the intensity, frequency and phase of the light to measure the signal. It can be used for measurements of the mechanical quantity, thermal quantity, electromagnetic quantity, medical, and atmospheric monitoring. Compared with the traditional sensors, optical fiber sensors have many merits, such as small size, anti-electromagnetic interference, high sensitivity, corrosion resistance, and so on.

In this thesis, we have concentrated our research works on the optimal design and fabrication of one of the fiber devices: the long-period fiber grating (LPG), especially for

the helical type LPGs, and explore its potential applications to the fields of fiber sensor and optical communication.

1.2 Applications of the fiber-grating based sensor

Fiber grating is a sensitive component with excellent performance, which can be used as sensors in various fields. The sensing mechanism can be summarized as that any changes of the temperature, stress, or strain in the external environment will inevitably bring some changes to the effective refractive-index of the mode, the grating period, and thus make the fiber grating resonance conditions change.

By measuring the change of the resonant wavelength of the grating, we can obtain the information of the surrounding environment parameters. The mechanism of the fiber gratings–based sensor includes temperature-induced deformation and the thermo-optic effect, strain-induced deformation and the elastic effect, Faraday effects caused by the applied magnetic field, and effective refractive index induced by the index of the surrounding materials. Based on these basic sensing mechanisms, this kind of sensors can naturally be used to measure stress, strain, temperature, acceleration, vibration, inclination, pressure, current, magnetic field, and refractive index of the surrounding materials. Precise measurements to these parameters are important and essential to the civil engineering, aerospace, marine exploration, petrochemical, power electronics industry, biomedical engineering, chemical engineering fields etc.

Comparing with the ordinary fiber-based sensor, fiber grating-based ones have their own unique advantages. Since the fiber gratings have their self-reference points compact size, and thus easily to be combined to form various types of sensing networks for large area distributed measurement, therefore, the fiber grating-based sensors are suitable for the cases under a strong electromagnetic field, or strong radiation, corrosive, any other dangerous and harsh environments. Especially available to the application of the real-time monitoring of multi-point measurements to bridges, dams, buildings, airplanes, ships, trains, mines and oil fields etc. Since 1989, the first time that the fiber grating-based strain and temperature sensor had been proposed by Morey et al. [1], many research institutes all over the world have paid much attention to it and have carried out a wide range of applied researches [2, 3]. To date, study for this kind of sensors has been expanded and has been

successfully applied in many fields. Some of their applications are described below.

I. Application in Geodynamics [4, 5]

The detection of seismic volcanoes is an important research topic in Geodynamics. For example, the detection of stress and temperature changes near the crater, is one of the most effective means of revealing the volcanic activity and evolution of the volcanoes itself. In order to know the exact location of the seismic or the volcano source, and in order to better describe the geometry and evolution of the source region, densely distributed stress-strain gauges are strongly required. Fiber grating-based sensor is a good selection which enables to provide in-line seismic detection with a long-distance dense array of sensor network. It can be used as terrain detectors or optical seismometers to detect the rock deformation and the vertical shock wave.

II. Applications to the spacecraft and ship [6]

The carbon fiber reinforced composite material has the advantages of good fatigue resistance and corrosion resistance, light weight and high mechanical performance, and can lighten the weight of hull or spacecraft, which is important for fast shipping and flying. Therefore, composite materials are increasingly used in the manufacture of aerospace tools.

To measure the condition of the hull, one needs to understand the different parts of the deformation torque, shear pressure, the deck suffered the attack, the general hull need nearly 100 sensors, and the fiber grating-based sensor with strong wavelength multiplexing capability is an ideal one for hull detection, it can be used to measure the internal stress of the hull, as well as the waves on the deck of the attack. In addition, multiple sensors are often required to monitor an aircraft for strain, temperature, vibration measurements under the conditions of taking off, landing, acceleration, and in ultrasonic fields. Attributed to characteristic of light weight, small size, and high spatial resolution, the fiber grating-based sensor embedded in the material becomes an ideal sensing component to realize multi-point, multi-axial and multi-parameter strain and temperature measurement in spacecraft.

III. Applications in civil engineering [7]

Fiber grating-based sensors also have many important applications to civil engineering for structural monitoring of such as the bridges, the mines, the tunnels, the dams, and some of the large buildings, etc. By measuring the strain distribution of the structure, one can predict the local structure of the load and the practical status, and thus helpful to decide when the maintenance and repair are necessary. In principle, fiber grating sensors can be attached to the surface of the structure or embedded in the middle of the structure, play key roles for the temperature monitoring, the shock detection, the deformation control, and the vibration detection in order to find probable defect in structure. In addition, multiple fiber grating sensors can easily be connected in series to form a sensing network, which is especially available to the structure of quasi-distributed detection by using the computer remote sensing system.

On the other hand, fiber grating sensors can be used for monitoring the bridges, the roads, and the railway systems. For examples, they had already been found applications in the Calgary Beddington Trail Bridge in Canada, the New Mexico Las Cruces on 10th Interstate Expressway, the 2160 meters long span of the Tsing Ma Bridge [8], and the China's Qinghai-Tibet Railway system. Especially for the last one, i.e., in the China's Qinghai-Tibet Railway system, there exists a large number of permafrost areas. Since the status of permafrost will considerably affect the safety of railway embankment, in the frozen soil of more than 500 observation points, fiber grating-based temperature sensors with accuracy of ±0.1℃ have been employed [9].

IV. Applications in electric power industry [10]

Fiber grating-based sensors are ideal sensing components in power industry, because they are immune to electromagnetic interference and the measured object, the optical signal can be transmitted over long distances with low losses. For examples, the fiber grating-based sensors can be used for measuring and monitoring the probable defects in the turbine blades, the transformer temperature, and the high current, and the load on a

high-voltage carried wire. For the last one case that a heavy load applied to the electric wires, such as the heavy snow case which may cause the electricity-breaking accidents, so it is very essential to measure and monitor the load-bearing pressure on the cable. However, it is very difficult to be realized for remote high-voltage mountain cables. Generally the high-voltage cables are supported in the middle by the two wires which are "insulator" made of glass fiber. To make fiber grating embedded in the same "insulator", one can measures the axial stress suffered and calculate the pressure on the high-voltage wire distribution, and thus enables to obtain timely warning for either replacement or the necessary maintenance.

Besides the long-range harsh environment measurement, the sensors where the fiber gratings are encapsulated in a piezoelectric ceramic and a magnetostrictive material have also been used to measure the magnetic field and current, respectively[11].

V. Applications in Medicine [12]

In many cases, such as partial medical procedures, the use of electronic sensors as detectors is not suitable, especially in high-frequency treatments such as high microwave radiation, ultrasound fields or laser radiation. In order to damage less to the human tissue or even harmless in vivo testing, small size of the sensor is essential to medical applications. Fiber grating-based sensors are much smaller than traditional electronic sensors. They can be used to measure the local temperature, pressure and sound-field information for the tissue of human body but with minimum invasion. At present, the fiber grating sensing system has successfully been used for detecting the temperature and ultrasonic field of the diseased tissue, and the measurement result with the resolution of 0.1℃ and the accuracy of ± 0.2℃ in the range of 30℃ -60℃, have been obtained, meanwhile the measurement resolution of 10^{-3}atm/Hz$^{1/2}$ for the ultrasonic field has been obtained also, which enable to provide useful information for the research of lesion tissue [13]. Fiber grating sensors can also be used to measure the efficiency of the heart. In this approach, a thermo-dilution catheter combined with a fiber grating was inserted into the right atrium of the patient's heart, where the temperature of the pulmonary arterial blood and the pulse power have been

measured in order to know the blood output of the heart.

In addition, to help doctors monitor the health of patients, the Nanyang Technological University Biomedical Engineering Research Center developed a fiber grating sensor for surgical correction, where they made use of the grating arrays as a mapping device to monitor the tibiae pressure. As result, the knee joint stretching movement of the pressure distribution can be monitored, which will be helpful to develop a prosthetic leg and thus satisfy the patient's actual needs [14].

VI. Applications in chemistry

Because the resonant wavelength of the fiber Bragg grating (FBG) and the loss-peak wavelength of the long-period fiber grating (LPG) both are very sensitive to the index-change of the external environment, these two kinds of grating especially the LPG-based sensor have been widely used for chemical sensing. In principle, the changes in the concentration of the surrounded chemical substances will bring out the changes in the effective index of the cladding mode, and thus results in a wavelength shift for the loss-peak. To date, LPG-based sensors have been used to measure the concentration of many chemical solutions including the sucrose, ethanol, hexanol, hexadecane, $CaCl_2$, NaCl and so on. As matter of fact, any chemical solution whose refractive index is less than 1.44 (the refractive index of the silica fiber) can be detected by using the LPG-based sensor.

1.3 Developments of the long period fiber grating

As one of the important fiber components, fiber grating has been widely applied to optical communication and fiber sensor system. To date, there are two kinds of fiber gratings: the fiber Bragg grating (FBG) which in generally has a period of sever hundred nanometers [15-19] and the long period fiber grating (LPG) which generally has a period of sever hundred micrometers [20-30]. Since Hill et al. [15] and Vengsarkar et al. [20] had proposed and demonstrated the first FBG and LPG in 1978 and 1996, respectively, the fabrications and applications of the in-fiber gratings have achieved rapid development. Up to time now, a lot of fabrication methods, such as the ultraviolet (UV) laser exposure [20-30], the CO_2 laser irradiation [31-43], the electric arc discharge [44-49], femtosecond laser exposure [50-56], mechanical micro-bends [57-62], etched corrugations [63-68], and the ion-beam implantation [69, 70], have been proposed and demonstrated to fabricate the LPGs with different kinds of optical fibers. After that, LPG-based devices have been numerically proposed to find their applications to the fields of fiber sensor and fiber communication [19, 29, 37].

In 1998, Davis et al. [31, 32] reported what is the first example of gratings fabricated by the CO_2 laser irradiation method in a conventional glass fiber. Compared with the UV-laser exposure method, the CO_2 laser irradiation method is much more flexible and low cost because no photosensitivity and any other pretreated process are required to fabricate a grating in the glass fibers [31-43]. Moreover, the CO_2 laser irradiation process can be controlled to write any complicated gratings without the expensive masks.

1.4 Applications of the long period fiber grating

It is well known that the loss-peak wavelength of the LPGs is very sensitive to the surrounding environmental parameters, such as the temperature, strain, bend, and the ambient refractive index. For the temperature measurement, in 1999 Kinm et al [68] firstly investigated the thermal performances of the LPG and proposed a new method to increase thermal sensitivity of LPG by using a specific fiber which has a high thermos-optical coefficient between core and cladding. In 2002, Khaliq et al [69] had proposed another method to increase the thermal sensitivity by coating a special material on the surface of the LPG, and as result, the temperature sensitivity of 19.2 nm/°C within the temperature range of 1.1°C was obtained.

Referring to the strain measurement, in 2006, Y.-P. Wang et al [38] developed a LPG strain sensor with a high strain sensitivity of -7.6 pm/με and a low temperature sensitivity of 3.91 pm/°C. In 2009, T. Zhu et al. [71] had proposed a temperature-independent strain sensor, which was demonstrated based on measuring the wavelength-separation change of the two loss-peaks in term of the ambient temperature, where the utilized LPG was written in a twisted optical fibers and as a result, a high strain sensitivity of 106.7 pm/με was obtained.

Referring to the LPG-based refractive-index sensor, principle of which is based on the fact that the effective refractive index of the cladding modes are strongly dependent on the refractive index of the surrounding medium. As a result of the phase-matching condition, the resonant wavelength (i.e., the loss peak wavelength) of LPG will largely changes whenever the index of the surrounding solutions have changes. To date, LPGs have been developed to realize various kinds of refractive-index sensors, such as the chemical concentration sensors [72-75], the liquid-level sensor [76], and the device used as a tunable filter in spectrum.

On the other hand, in the field of optical communication, the long period fiber grating is a very good transmission band-stop filter with advantages of the low loss, without

backward reflection, electromagnetic interference-free, and the compatibility with the optical fiber. Moreover, stop-band of the LPG is much broader than that of the FBG devices.

LPG had also been used as a gain flatten filter used for Erbium-doped fiber amplifier (EDFA), which probably be the most featured application of LPG in optical communication field [77]. A. M. Vengsarkar et al [77] firstly proposed the LPG based gain flattener by making two different LPGs cascaded, as a result, a flattened EDFA spectrum with a bandwidth of 25 ~ 30nm and unevenness less than 0.2dB had been successfully obtained.

In LPG, the fundamental core-mode at the resonant wavelength can be coupled (transferred) into the cladding and propagates forward in the cladding, and meanwhile the resulted cladding mode can also be coupled back to the core mode when it encounters another LPG but with the same period. Because the optical path produced by the core mode and cladding mode are different, the Mach-Zehnder interference phenomenon could happen once if two parts of the lights meets again, which can result in a spectrum with multiple band-pass filter structures. X. J. Gu [78] and C. D. Su [79] had firstly proposed this structures for realization of the multi-wavelength band-pass filter and multi-wavelength fiber light source.

1.5 Overview of this thesis

In this thesis, we concentrate our research works on the design and fabrication of the advanced LPG: helical-type of LPG and its applications to fiber sensor and fiber communication fields. The main objective for moving to helical long period fiber grating (HLPG) technique is due to its following benefits discussed. Firstly, the obtained HLPG and its spectrum have a high repeatability with the attenuation peak at a particular wavelength. Secondly, the entire experimental setup and methodology used is extremely simple and cost effective. Thirdly, the robust nature of the fabricated HLPG makes it possible to measure a wide range of sensitivity (Torsion sensor, strain sensors, bending sensor, and so on) which is hardly realized using the conventional long period grating (LPG). Last but not the least, because it`s helical and symmetric structure which made us likely to realize twist sensor with this kind of gratings.

In Chapter 1, a brief introduction about the basic techniques of fiber gratings is given, which includes the classification, fabrication, and application of the LPGs in sensing region and optical communication region.

In Chapter 2, firstly, characteristics of the conventional optical fiber are reviewed in details. Secondly, theory of the LPG based on the coupled mode theory and transfer matrix method is introduced.

In Chapter 3, firstly, we propose and successfully demonstrate a CO_2 laser irradiation method to write the long period fiber grating. Secondly, we fabricate and experimentally investigate several kinds of phase-shifted LPGs, where both the grating and the inserted phase-shift are obtained simultaneously by using CO_2 laser irradiation method. Moreover, with a π phase-shifted LPG being particularly used, a robust temperature-insensitive sensor that allows for large strain measurement up to 7600 με was proposed and successfully demonstrated.

In Chapter 4, firstly we propose a new-type of LPG which has helical structure in the fiber. Secondly, this new kind of HLPG written by using CO_2 laser technique is experimentally demonstrated, where a sapphire tube is particularly utilized in place of the

focal lens. Thirdly, we also carry out the theoretical analysis to HLPG based on the mode-coupling theory.

In Chapter 5, we explore the application of the helical LPG. This is the first report to fabricate the HLPGs with this technique. The proposed method allows us to well fabricate HLPGs even with a diameter less than several tens of micrometer. In order to compare with the experimental results, theoretical simulations have also been done, which are related to changes of the resonant wavelengths of HLPGs under the condition of three different fiber diameters. As an application of this kind of HLPGs, a novel HLPGs-based refractometric sensor that allows for temperature-free measurement of the refractive index is proposed and experimentally demonstrated.

In Chapter 6, we propose and demonstrate a novel method for the fabrication of flat-top band-rejection, which is realized by fabricating two HLPGs but with opposite helicities with using CO_2 laser and the sapphire tube technique and successively cascading these two LPGs. The proposed HLPGs have a relative short length (less than 4.6 cm) and do not require a complex apodization in grating's amplitude, which make this kind of HLPGs particularly suitable be fabricated by using the robust CO_2 laser writing technique.

References

[1]. W. W. Morey, G. Meltz and W. H. Glenn, “Fiber optic Bragg grating sensors,” Proc. SPIE, 1169, 98 (1989).

[2]. A. D. Kersey, M. A. Davis, H. J. Patrick, et al., “Fiber grating sensors,” J. Lightwave. Technol, 15(8), 1442 (1997).

[3]. R. Willsch, “Application of optical fiber sensors: technical and market trends,” Proc. SPIE, 4074, 24 (2000).

[4]. Y. Zhang, S.G. Li, Z.F. Yin, B.Q. Chen, and H.-L. Cui, “Fiber-Bragg-grating-based seismic geophone for oil/gas prospecting,” Opt. Eng., 45(8), 084404 (2006).

[5]. A. Laudati, F. Mennella, M. Giordano, G. D`Altrui, C.C. Tassini and A. Cusano, “A fiber-optic Bragg grating seismic sensor,” IEEE Photon. Technol. Lett., 19(24), 1991 (2007).

[6]. P. Foote, I. Read, “Applications of optical fiber sensors in aerospace: the achievements and challenges,” Proc. SPIE, 4074, 246 (2000).

[7]. H. W. Cai, Z. P. Xia, J. X. Geng et al, “Fiber grating sensors system for civil structural stain monitoring,” Proc. SPIE, 5279, 450 (2004).

[8]. Http://www.tkyb.com/cpyy.htm

[9]. M. Akira, Y. Isamu, “Fiber Bragg grating accelerometer for buildings and civil infrastructures,” Proc. SPIE, 4330, 479 (2001).

[10]. P. Niewczas, L. Dziuda, G. Fusiek et al., “Design and evaluation of a pre-protype hybrid fiber-optic voltae sensor for a remotely interrogated condition monitoring system,” IEEE Instrumentation and Measurement Technology Conference, 3, 2369 (2004).

[11]. B. Yi, B. C. B. chu, and K. S. Chiang, “Temperature compensation for a Fiber-Bragg-Grating-Based magnetostrictive sensor,” Microwave and Optical Technol. Lett., 42, 1906 (2003).

[12]. D. J. Webb, Y. J. Rap, M. W. Hathaway et al., “Medical temperature profile monitoring using multiplexed fiber Bragg gratings,” Proc. SPIE, 3541, 256 (1998).

[13]. N. E. Fisher D. J. Webb, C. N. Pannell et al., “Medical ultrasound detection using fiber Bragg gratings,” Proc. SPIE, 3541, 27 (1998).

[14]. L. Mohanty, S. C. Tjin, D. T.T. Lie, S. E.C. Panganiban and P. K.H. Chow, “Fiber grating sensor for pressure mapping during total knee arthroplasty,” Sensors and Actuators A: Physical, 135(2), 323 (2007).

[15]. K. O. Hill, Y. Fujii, D. C. Johnson, and B. S. Kawasaki, “Photosensitivity in optical fiber waveguides: Application to reflection filter fabrication,” Appl. Phys. Lett. 32, 647 (1978).

[16]. Y.-J. Rao, “In-fiber Bragg grating sensors,” Meas. Sci. Technol. 8, 355 (1997).

[17]. Y. J. Rao, “Recent progress in applications of in-fibre Bragg grating sensors,” Opt. Lasers Eng. 31, 297 (1999).

[18]. D. Kersey, M. A. Davis, H. J. Patrick, M. LeBlanc, K. P. Koo, C. G. Askins, M. A. Putnam, and E. J. Friebele, “Fiber grating sensors,” J. Lightwave Technol. 15, 1442 (1997).

[19]. M. Vengsarkar, P. J. Lemaire, J. B. Judkins, V. Bhatia, T. Erdogan, and J. E. Sipe, “Long-period fiber-grating as band-rejection filters,” J. Lightwave Technol. 14, 58 (1996).

[20]. M. Vengsarkar, P. J. Lemaire, J. B. Judkins, V. Bhatia, T. Erdogan, and J. E. Sipe, “Long-period fiber-grating-based gain equalizers,” J. Lightwave Technol. 14, 58 (1996).

[21]. V. Bhatia and A. M. Vengsarkar, “Optical fiber long-period grating sensors,” Opt. Lett. 21, 692 (1996).

[22]. T. Erdogan, “Fiber grating spectra,” J. Lightwave Technol. 15, 1277 (1997).

[23]. T. Erdogan, “Cladding-mode resonance in short- and long-period fiber grating filter,” J. Opt. Soc. Am. A 14, 1760 (1997).

[24]. T. Erdogan, “Cladding-mode resonance in short- and long-period fiber grating filter: errata,” J. Opt. Soc. Am. A 17, 2113 (2000).

[25]. B. J. Eggleton, R. E. Slusher, J. B. Judkins, J. B. Stark, and A. M. Vengsarkar,”

All-optical switching in long-period fiber gratings," Opt. Lett. **22**, 883 (1997).

[26]. B. J. Eggleton, P. S. Westbrook, R. S. Windeler, S. Spalter, and T. A. Strasser," Grating resonances in air-silica microstructured optical fibers" Opt. Lett. 24, 1460 (1999).

[27]. B. J. Eggleton, P. S. Westbrook, C. A. White, C. Kerbage, R. S. Windeler, and G. L. Burdge, "Cladding mode resonances in air-silica microstructur optical fibers" J. Lightwave Technol. 18, 1084 (2000).

[28]. S. W. James and R. P. Tatam, "Optical fibre long-period grating sensors: characteristics and application," Meas. Sci. Technol. 14, R49 (2003).

[29]. V. Bhatia, "Applications of long-period gratings to single and multi-parameter sensing," Opt. Express 4, 457 (1999).

[30]. D. D. Davis, T. K. Gaylord, E. N. Glytsis, S. G. Kosinski, S. C. Mettler, and A. M. Vengsarkar, "Optical-fiber-to-waveguide coupling using carbon-dioxide-laser-induced long-period fiber gratings," Electron. Lett. 34, 302 (1998).

[31]. D. D. Davis, T. K. Gaylord, E. N. Glytsis, and S. C. Mettler, "CO_2 laser-induced long-period fibre gratings: spectral characteristics, cladding modes and polarisation independence," Electron. Lett. 34, 1416 (1998).

[32]. D. D. Davis, T. K. Gaylord, E. N. Glytsis, and S. C. Mettler, "very-high-temperature stable CO_2-laser-induced long-period fiber gratings," Electron. Lett. 35, 740 (1999).

[33]. G. Kakarantzas, T. E. Dimmick, T. A. Birks, R. Le Roux, and P. S. J. Russell, "Miniature all-fiber devices based on CO 2 laser microstructuring of tapered fibers," Opt. Lett. 26, 1137 (2001).

[34]. G. Kakarantzas, T. A. Birks, and P. S. Russell, "Structural long-period gratings in photonic crystal fibers," Opt. Lett. 27, 1013 (2002).

[35]. Y.-J. Rao, Y.-P. Wang, Z.-L. Ran, and T. Zhu, "Novel Fiber-Optic Sensors Based on Long-Period Fiber Gratings Written by High-Frequency CO 2 Laser Pulses," J. Lightwave Technol. 21, 1320 (2003).

[36]. Y. J. Rao, T. Zhu, Z. L. Ran, Y. P. Wang, J. Jiang, and A. Z. Hu, "Novel long-period

fiber gratings written by high-frequency CO_2 laser pulses and applications in optical fiber communication," Opt. Commun. 229, 209 (2004).

[37]. Y.-P. Wang, D. N. Wang, W. Jin, Y.-J. Rao, and G.-D. Peng, "Asymmetric long period fiber gratings fabricated by use of CO 2 laser to carve periodic grooves on the optical fiber," Appl. Phys. Lett. 89, 151105 (2006).

[38]. Y.-P. Wang, L. M. Xiao, D. N. Wang, and W. Jin, "Highly sensitive long-period fiber-grating strain sensor with low temperature sensitivity," Opt. Lett. 31, 3414 (2006).

[39]. Y. Wang, L. Xiao, D. N. Wang, and W. Jin, "In-fiber polarizer based on a long-period fiber grating written on photonic crystal fiber," Opt. Lett. 32, 1035 (2007).

[40]. Y. Wang, W. Jin, J. Ju, H. Xuan, H. L. Ho, L. Xiao, and D. Wang, "Long period gratings in air-core photonic bandgap fibers" Opt. Express 16, 2784 (2008).

[41]. Y. Zhu, P. Shum, J.-H. Chong, M. K. Rao, and C. Lu, "Deep-notch, ultracompact long-period grating in a large-mode-area photonic crystal fiber" Opt. Lett. 28, 2467 (2003).

[42]. Y. N. Zhu, P. Shum, H.-W. Bay, X. Y. Chen, C.-H. Tan, and C. Lu, "Wide-passband, temperature-insensitive, and compact π-phase-shifted long-period gratings in endlessly single-mode photonic crystal fiber," Opt. Lett. 29, 2608 (2004).

[43]. I. K. Hwang, S. H. Yun, and B. Y. Kim, "Long-period fiber gratings based on periodic microbends," Opt. Lett. 24, 1263 (1999).

[44]. J. S. Petrovic, H. Dobb, V. K. Mezentsev, K. Kalli, D. J. Webb, and I. Bennion, "Sensitivity of LPGs in PCFs Fabricated by an Electric Arc to Temperature, Strain, and External Refractive Index," J. Lightwave Technol. 25, 1306 (2007).

[45]. G. Humbert, A. Malki, S. Fevrier, P. Roy, and D. Pagnoux, "Characterizations at high temperatures of long-period gratings written in germanium-free air–silica microstructure fiber," Electron. Lett. 39, 349 (2003).

[46]. H. Dobb, K. Kalli, and D. J. Webb, "Temperature-insensitive long period grating sensors in photonic crystal fiber," Electron. Lett. 40, 657 (2004).

[47]. G. Rego, P. V. S. Marques, H. M. Salgado, and J. L. Santos, “Simultaneous measurement of temperature and strain based on arc-induced long-period fiber gratings,” Electron. Lett. 41, 60 (2005).

[48]. G. M. Rego, J. L. Santos, and H. M. Salgado, “Polarization dependent loss of arc-induced long-period fiber gratings,” Opt. Commun. 262, 152 (2006).

[49]. Y. Kondo, K. Nouchi, T. Mitsuyu, M. Watanabe, P. G. Kazansky, and K. Hirao, “Fabrication of long-period fiber gratings by focused irradiation of infrared femtosecond laser pulses,” Opt. Lett. 24, 646 (1999).

[50]. E. Fertein, C. Przygodzki, H. Delbarre, A. Hidayat, M. Douay, and P. Niay, “Refractive-index changes of standard telecommunication fiber through exposure to femtosecond laser pulses at 810 cm,” Appl. Opt. 40, 3506 (2001).

[51]. 40A. Martinez, M. Dubov, I. Khrushchev, and I. Bennion, “Direct writing of fiber Bragg gratings by femtosecond laser,” Electron. Lett. 40, 1170 (2004).

[52]. L. B. Fu, G. D. Marshall, J. A. Bolger, P. Steinvurzel, E. C. Magi, M. J. Withford, and B. J. Eggleton, “Femtosecond laser writing Bragg gratings in pure silica photonic crystal fibers,” Electron. Lett. 41, 638 (2005).

[53]. D. Grobnic, S. J. Mihailov, C. W. Smelser, M. Becker, and M. W. Rothhardt, “Femtosecond laser fabrication of Bragg gratings in borosilicate ion-exchange waveguides,” IEEE Photonics Technol. Lett. 18, 1403 (2006).

[54]. S. J. Mihailov, D. Grobnic, D. Huimin, C. W. Smelser, and B. Jes, “Femtosecond IR laser fabrication of Bragg gratings in photonic crystal fibers and tapers,” IEEE Photonics Technol. Lett. 18, 1837 (2006).

[55]. S. Savin, M. J. F. Digonnet, G. S. Kino, and H. J. Shaw, “Tunable mechanically induced long-period fiber gratings,” Opt. Lett. 25, 710 (2000).

[56]. J. Y. Cho and K. S. Lee, “A birefringence compensation method for mechanically induced long-period fiber gratings,” Opt. Commun. 213, 281 (2002).

[57]. G. Rego, “Polarization dependent loss of mechanically induced long-period fibre gratings,” Opt. Commun. 281, 255 (2008).

[58]. T. L. S, N. A. George, P. Sureshkumar, P. Radhakrishnan, C. P. G. Vallabhan, and V. P. N. Nampoori, “Chemical sensing with microbent optical fiber,” Opt. Lett. 26, 1541 (2001).

[59]. P. Steinvurzel, E. D. Moore, E. C. Magi, B. T. Kuhlmey, and B. J. Eggleton, “Long period grating resonances in photonic bandgap fiber,” Opt. Express 14, 3007 (2006).

[60]. L. Su, K. S. Chiang, and C. Lu, “Microbend-induced mode coupling in a graded-index multimode fiber,” Appl. Opt. 44, 7394 (2005).

[61]. C. Y. Lin and L. A. Wang, “Loss-tunable long period fibre grating made from etched corrugation structure,” Electron. Lett. 35, 1872 (1999).

[62]. C. Y. Lin and L. A. Wang, “A wavelength-and loss-tunable band-rejection filter based on corrugated long-period fiber grating,” IEEE Photonics Technol. Lett. 13, 332 (2001).

[63]. C. Y. Lin, L. A. Wang, and G. W. Chern, “Corrugated long-period fiber gratings as strain, torsion, and bending sensors,” J. Lightwave Technol. 19, 1159 (2001).

[64]. C.-Y. Lin, G.-W. Chern, and L. A. Wang, “Periodical corrugated structure for forming sampled fiber Bragg grating and long-period fiber grating with tunable coupling strength,” J. Lightwave Tech. 19, 1212 (2001).

[65]. J. Yan, L. Qun, L. Chien-Hung, E. Lyons, I. Tomov, and H. P. Lee, “A novel strain-induced thermally tuned long-period fiber grating fabricated on a periodic corrugated silicon fixture,” IEEE Photonics Technol. Lett. 14, 941 (2002).

[66]. M. Fujimaki, Y. Ohki, J. L. Brebner, and S. Roorda, “Fabrication of long-period optical fiber gratings by use of ion implantation,” Opt. Lett. 25, 88 (2000).

[67]. M. L. von Bibra, A. Roberts, and J. Canning, “Fabrication of long-period fiber gratings by use of focused ion-beam irradiation,” Opt. Lett. 26, 765 (2001).

[68]. C. S. Kinm, Y. G. Han, J. N. Kim, et al, “Enhancement and suppression of the thermal sensitivity of long period fiber gratings fabricated with a CO_2 laser,” CLEO. 131-132 (1999).

[69]. S. Khaliq, S. W. James, and R. P. Tatam, “Enhanced sensitivity fiber optic long period

grating temperature sensor," Meas. Sic. Technol. 13, 792-795 (2002).

[70]. T. Zhu, Y.-J. Rao, Y. Song, K. S. Chiang, and M. Liu, "Highly sensitive temperature-independent strain sensor based on a long-period fiber grating with a CO_2-laser engraved rotary structure," IEEE Photonics Technol. Lett. 21, 543-545 (2009).

[71]. H J, Patrick, A. D. Kersey, and F, Bucholtz, "Analysis of the response of long period fiber gratings to external index of refraction," J. Lightwave Technol. 16, 1606–42 (1998).

[72]. Shu X and Huang D, "Highly sensitive chemical sensor based on the measurement of the separation of dual resonant peaks in a 100 μm period fiber grating," Opt. Commun. 171, 65–9 (1999).

[73]. Allsop T, Zhang L and Bennion I, "Detection of organic aromatic compounds by a long period fiber grating optical sensor with optimised sensitivity," Opt. Commun. 191, 181–90 (2001).

[74]. Falciai R, Mignani A G and Vannini A, "Long period gratings as solution concentration sensors," Sensors Actuators B 74, 74–77 (2001).

[75]. Khaliq S, James S W and Tatam R P, "Fiber-optic liquid level sensor using a long-period grating," Opt. Lett. 26, 1224–6 (2001).

[76]. A. M. Vengsarkar, J. R. Pedrazzani, J. B. Judkins, and P. J. Lemaire, "Long-period fiber-grating-based gain equalizers," Opt. Lett. 21, 336-338 (1996).

[77]. X. J. Gu, "Wavelength-division multiplexing isolation fiber filter and light source using cascaded long-period fiber grating," Opt. Lett. 23, 509-510 (1998).

[78]. C. D. Su, and L. A. Wang," Multiwavelength fiber source by using long period fiber gratings in superfluorescent fiber source," Electron. Lett. 35, 927-929 (1999).

2. Mode theory in an optical fiber

2.1 Basic characteristics of the optical fiber

The basic structural characteristics of the optical fiber for communication are core diameter, cladding diameter, eccentricity of the core, and refractive-index difference. The basic transmission characteristics include the transmission band and transmission loss. Sometimes we use the numerical aperture (NA) instead of the refractive-index difference. Figure 2.1.1 shows the structure of an optical fiber where the core diameter of 2a, the cladding diameter of 2b, the core refractive-index n_1, the cladding refractive-index n_2 are assumed. Relation between the critical angle $\theta_c$of the fiber, the maximum acceptance angle θ_m, and the numerical aperture (NA) is given by

$$NA = \sin\theta_m = n_1 \sin\theta_c = \sqrt{n_1^2 - n_2^2}. \quad (2.1.1)$$

It is only a function of the core and clad's refractive-index. Usually, the difference of n_1 and n_2 is less than 1%, the relative refractive-index difference Δ is

$$\Delta = (n_1 - n_2)/n. \quad (2.1.2)$$

When the $n_1 \approx n_2$, NA is

$$NA = n_1\sqrt{2\Delta}. \quad (2.1.3)$$

The refractive index of core n_1 is higher than that of the cladding n_2. Therefore the light beam that is coupled to the end face of the waveguide is confined in the core by total internal reflection. This structure is called optical wave guide, the light propagating through the optical fiber is called guided wave. Any kinds of electric field probably existed in the

transverse plane of the fiber are called the guided modes. The guided mode is called TE mode when the electric field is only existed in the transverse plane of the propagation direction. Correspondingly, the TM mode is that magnetic field is only existed in the transverse plane of the propagation direction.

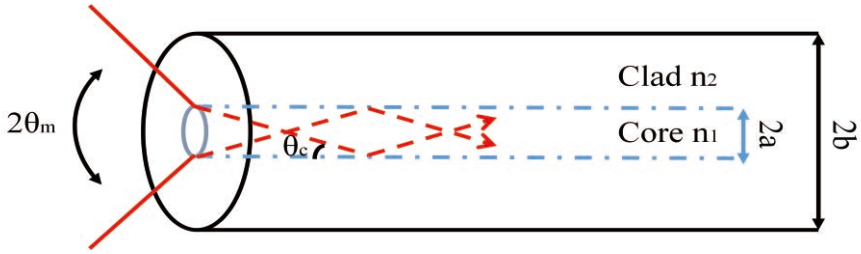

Fig. 2.1.1. Basic structure of the optical fiber

2.2 Mode dispersion equation

The dispersion equation is indispensable for knowing the transmission characteristics of the optical fiber and is obtained by solving Maxwell's equations. In this section, we analyze the step index type single mode fiber used in this research.

Firstly, we use Maxwell equation

$$\nabla \times \tilde{E} = -\mu_0 \frac{\partial \tilde{H}}{\partial t} \tag{2.2.1a}$$

$$\nabla \times \tilde{H} = \varepsilon_0 n^2 \frac{\partial \tilde{E}}{\partial t}. \tag{2.2.1b}$$

And the plane wave of cylindrical coordinate system is like

$$\tilde{E} = E(r,\theta)\exp\ j(\omega t - \beta z) \tag{2.2.2a}$$

$$\tilde{H} = H(r,\theta)\exp j(\omega t - \beta z). \tag{2.2.2b}$$

We substitute the equation (2.2.1) in equation (2.2.2):

$$\frac{\partial^2 E_z}{\partial r^2} + \frac{1}{r}\frac{\partial E_z}{\partial r} + \frac{1}{r^2}\frac{\partial^2 E_z}{\partial \theta^2} + [k^2 n(r,\theta)^2 - \beta^2]E_z = 0 \tag{2.2.3a}$$

$$\frac{\partial^2 H_z}{\partial r^2} + \frac{1}{r}\frac{\partial H_z}{\partial r} + \frac{1}{r^2}\frac{\partial^2 H_z}{\partial \theta^2} + [k^2 n(r,\theta)^2 - \beta^2]H_z = 0. \tag{2.2.3b}$$

In the case of the axisymmetric optical fiber, since the waveguide structure in the θ direction has no nonuniformity, the refractive index distribution can be set to $n(r)$. At this time, the transverse component of the electromagnetic field can be expressed as follows

$$E_r = -\frac{j}{[k^2 n(r)^2 - \beta^2]}\left(\beta\frac{\partial E_z}{\partial r} + \frac{\omega\mu_0}{r}\frac{\partial H_z}{\partial \theta}\right) \tag{2.2.4a}$$

$$E_\theta = -\frac{j}{[k^2 n(r)^2 - \beta^2]}\left(\frac{\beta}{r}\frac{\partial E_z}{\partial \theta} - \omega\mu_0\frac{\partial H_z}{\partial r}\right) \tag{2.2.4b}$$

$$H_r = -\frac{j}{[k^2 n(r)^2 - \beta^2]}\left(\beta\frac{\partial H_z}{\partial r} - \frac{\omega\varepsilon_0 n(r)^2}{r}\frac{\partial E_z}{\partial \theta}\right) \quad (2.2.4c)$$

$$H_\theta = -\frac{j}{[k^2 n(r)^2 - \beta^2]}\left(\frac{\beta}{r}\frac{\partial H_z}{\partial \theta} + \omega\varepsilon_0 n(r)^2\frac{\partial E_z}{\partial r}\right). \quad (2.2.4d)$$

The θ dependence of the electromagnetic field distribution of the axisymmetric optical fiber is cos(nθ + φ) or sin(nθ + φ) (n is an integer, φ is a constant). The electromagnetic field mode of the optical fiber consists of the TE mode, the TM mode, and the hybrid mode.

In this section, for the sake of simplicity, calculate only for TE mode. The magnetic field distribution in the core and the cladding,

$$H_z = \begin{Bmatrix} g(r) \\ h(r) \end{Bmatrix}\cos(n\theta + \varphi) \quad \begin{matrix} (0 \le r \le a) \\ (r > a) \end{matrix} \quad . \quad \begin{matrix} (2.2.5a) \\ (2.2.5b) \end{matrix}$$

E(z) = 0, we substitute equation (2.2.3b) in equation (2.2.5a),

$$\frac{\partial^2 H_z}{\partial r^2} + \frac{1}{r}\frac{\partial H_z}{\partial r} + \frac{1}{r^2}\frac{\partial^2}{\partial \theta^2}(g(r)\cos(n\theta + \varphi)) + [k^2 n(r,\theta)^2 - \beta^2]H_z = 0$$

$$\frac{\partial^2 H_z}{\partial r^2} + \frac{1}{r}\frac{\partial H_z}{\partial r} + \frac{n^2}{r^2}(g(r)\cos(n\theta + \varphi)) + [k^2 n(r,\theta)^2 - \beta^2]H_z = 0$$

$$\frac{\partial^2 H_z}{\partial r^2} + \frac{1}{r}\frac{\partial H_z}{\partial r} + \left[k^2 n(r)^2 - \beta^2 - \frac{n^2}{r^2}\right]H_z = 0. \quad (2.2.6)$$

Since r = a and the magnetic field is continuous, from the boundary condition in the longitudinal direction (Hz) of the magnetic field

$$g(a)\ \cos(n\theta + \varphi) = h(a)\ \cos(n\theta + \varphi)$$

$$g(a) = h(a). \tag{2.2.7a}$$

From the boundary condition of the magnetic field in the horizontal direction, the (H_θ) can express by

$$-\frac{j}{[k^2 {n_1}^2 - \beta^2]}\left(\frac{\beta}{a} g(a)\sin(n\theta + \varphi)\right) = -\frac{j}{[k^2 {n_0}^2 - \beta^2]}\left(\frac{\beta}{a} h(a)\sin(n\theta + \varphi)\right), \tag{2.2.7b}$$

n_1 and n_2 are refractive indices of the core and cladding, respectively. In order for equation (2.2.7b) to hold for any θ, n = 0 must be satisfied. Therefore, $\partial / \partial\theta = 0$, and from equations (2.2.4a) and (2.2.4d)

$$E_r = H_\theta = 0. \tag{2.2.8}$$

When n = 0, the equation (2.2.4) and (2.2.6) are

$$\frac{\partial^2 H_z}{\partial r^2} + \frac{1}{r}\frac{\partial H_z}{\partial r} + [k^2 n(r)^2 - \beta^2]H_z = 0 \tag{2.2.9}$$

But

$$E_\theta = \frac{j\omega\mu_0}{[k^2 n(r)^2 - \beta^2]}\left(\frac{\partial H_z}{\partial r}\right) \tag{2.2.10a}$$

$$H_r = -\frac{j\beta}{[k^2 n(r)^2 - \beta^2]}\left(\frac{\partial H_z}{\partial r}\right) \tag{2.2.10b}$$

$$E_r = H_\theta = 0. \tag{2.2.10c}$$

Here, the wave number (transverse wave number) in the r direction of the core and the cladding is defined as follows

$$\chi = \sqrt{k^2 {n_1}^2 - \beta^2} \tag{2.2.11a}$$

$$\sigma = \sqrt{\beta^2 - k^2 {n_0}^2}. \tag{2.2.11b}$$

In order for light propagated in the core, $n_0 \leq \beta/k \ll n_1$, β/k is called the effective (equivalent) refractive index, and is the refractive index felt by the light when propagating through the fiber.

At this time, the wave equation of the core is $H_z = g(r)$, following by

$$\frac{\partial^2 g}{\partial r^2} + \frac{1}{r}\frac{\partial g}{\partial r} + \chi^2 g = 0, \tag{2.2.12}$$

and the wave equation of the cladding is $H_z = h(r)$, following by

$$\frac{\partial^2 h}{\partial r^2} + \frac{1}{r}\frac{\partial h}{\partial r} - \sigma^2 g = 0. \tag{2.2.13}$$

The solution of equation (2.2.12) is the zero order Bessel function $J_0(\chi r)$ or the Neumann function $N_0(\chi r)$. However, $N_0(\chi r)$ is not appropriate because it diverges to minus infinity at r=0. In addition, the solution of Eq. (2.2.13) is the zero-order first-order deformable Bessel function $K_0(\sigma r)$ or the second kind modified Bessel function $I_0(\sigma r)$, but $I_0(\sigma r)$ plus infinity at r = ∞ It diverges and is inappropriate. Finally, the solution of TE mode

$$H_z = \begin{cases} AJ_0(\chi r) & (0 \leq r \leq a) \\ BK_0(\sigma r) & (r > a) \end{cases}. \tag{2.2.14a}$$
$$\tag{2.2.14b}$$

From the boundary condition of the electromagnetic field (H_z, E_θ) in these functions

$$AJ_0(\chi a) = BK_0(\sigma a) \tag{2.2.15a}$$

$$\frac{j\omega\mu_0}{[k^2 n(r)^2 - \beta^2]}\left(\frac{\partial}{\partial r}AJ_0(\chi r)\right) = \frac{j\omega\mu_0}{[k^2 n(r)^2 - \beta^2]}\left(\frac{\partial}{\partial r}BK_0(\sigma r)\right)$$

$$\frac{A}{\chi}J_0{}'(\chi a) = -\frac{B}{\sigma}K_0{}'(\sigma r), \tag{2.2.15b}$$

where, the new parameters are

$$u = \chi a = a\sqrt{k^2 {n_1}^2 - \beta^2} \tag{2.2.16a}$$

$$w = \sigma a = a\sqrt{\beta^2 - k^2 {n_0}^2}. \tag{2.2.16b}$$

We use the equation

$$\frac{J_1(u)}{uJ_0(u)} = \frac{K_1(\omega)}{\omega K_0(\omega)}, \tag{2.2.17}$$

to solve the equation (2.2.15),

$$\frac{J_0{}'(u)}{uJ_0(u)} = -\frac{K_0{}'(w)}{wK_0(w)}. \tag{2.2.18}$$

This is the dispersion equation of TE mode. Therefore we use the property of Bessel`s function (($J_0{}'(u) = -J_1(u)$、 $K_0{}'(w) = -K_1(w)$) to get

$$\frac{J_1(u)}{uJ_0(u)} = -\frac{K_1(w)}{wK_0(w)}. \tag{2.2.19}$$

The equation (2.2.17) have a relationship follows

$$u^2 + w^2 = k^2({n_1}^2 - {n_0}^2)a^2 = v^2. \tag{2.2.20}$$

Given the normalized frequency v, the propagation constant can be obtained from the equations (2.2.19) and (2.2.20). The normalized frequency is a parameter that gives the propagation characteristics of an optical waveguide such as a fiber. In particular, it is used in discussing modes present in the waveguide.

$$v = kn_1 a\sqrt{\frac{{n_1}^2 - {n_0}^2}{{n_1}^2}} = \frac{2\pi a}{\lambda}\sqrt{{n_1}^2 - {n_0}^2}. \tag{2.2.21}$$

A single mode condition in which only the fundamental mode (HE_{11}^{co}mode) propagates through the optical fiber,

$$v < 2.405. \tag{2.2.22}$$

Finally, the electromagnetic field in the TE mode is obtained by substituting (2.2.14) into equation (2.2.10) and rearranging it using the properties of Bessel function.
In the core ($0 \le r \le a$)

$$\begin{aligned} E_\theta &= \frac{j\omega\mu_0}{[k^2 n(r)^2 - \beta^2]}\left(\frac{\partial}{\partial r} A J_0(\chi r)\right) \\ &= \frac{j\omega\mu_0}{\chi^2}\left(A {J_0}'\left(\frac{u}{a}r\right)\cdot\chi\right) \\ &= -j\omega\mu_0\frac{a}{u}A J_1\left(\frac{u}{a}r\right) \end{aligned} \tag{2.2.23a}$$

$$\begin{aligned} H_r &= -\frac{j\beta}{[k^2 n(r)^2 - \beta^2]}\left(\frac{\partial}{\partial r} A J_0(\chi r)\right) \\ &= -\frac{j\beta}{\chi^2}\left(A {J_0}'\left(\frac{u}{a}r\right)\cdot\chi\right) \\ &= j\beta\frac{a}{u}A J_1\left(\frac{u}{a}r\right) \end{aligned} \tag{2.2.23b}$$

$$H_z = A J_0\left(\frac{u}{a}r\right). \tag{2.2.23c}$$

In cladding ($r > a$)

$$E_\theta = \frac{j\omega\mu_0}{[k^2 n(r)^2 - \beta^2]}\left(\frac{\partial}{\partial r} BK_0(\sigma r)\right)$$

$$= \frac{j\omega\mu_0}{-\sigma^2}(BK_0{}'(\sigma r)\cdot\sigma)$$

$$= -j\omega\mu_0 \frac{a}{w}\left(-\frac{\sigma}{\chi} AJ_0{}'\left(\frac{u}{a}r\right)\right)$$

$$= -j\omega\mu_0 \frac{a}{w}\frac{\sigma}{\chi} AJ_1\left(\frac{u}{a}r\right)$$

$$= -j\omega\mu_0 \frac{a}{w}\frac{\sigma}{\chi}\left(-\frac{uJ_0(u)}{wK_0(w)} AK_1\left(\frac{w}{a}r\right)\right)$$

$$= j\omega\mu_0 \frac{a}{w}\frac{J_0(u)}{K_0(w)} AK_1\left(\frac{w}{a}r\right) \qquad (2.2.24a)$$

$$H_r = -\frac{j\beta}{[k^2 n(r)^2 - \beta^2]}\left(\frac{\partial}{\partial r} BK_0(\sigma r)\right)$$

$$= -\frac{j\beta}{-\sigma^2}(BK_0{}'(\sigma r)\cdot\sigma)$$

$$= j\beta \frac{a}{w}\left(\frac{\sigma}{\chi} AJ_1\left(\frac{u}{a}r\right)\right)$$

$$= j\beta \frac{a}{w}\frac{\sigma}{\chi}\left(-\frac{uJ_0(u)}{wK_0(w)} AK_1\left(\frac{w}{a}r\right)\right)$$

$$= -j\beta \frac{a}{w}\frac{J_0(u)}{K_0(w)} AK_1\left(\frac{w}{a}r\right) \qquad (2.2.24b)$$

$$H_z = BK_0\left(\frac{w}{a}r\right)$$

$$= \frac{J_0(u)}{K_0(w)} AK_0\left(\frac{w}{a}r\right). \qquad (2.2.24c)$$

Similarly to the TE mode, the dispersion equations in the TM mode and the hybrid mode can be solved, and for all these modes, it can be represented by the following general expression.

$$\frac{J_m(u)}{uJ_{m-1}(u)} = -\frac{K_m(w)}{wK_{m-1}(w)} \qquad (2.2.25)$$

But,

$$m = \begin{cases} 1 & \text{(TE mode and TM mode)} \quad (2.2.26a) \\ n+1 & \text{(EH mode)} \quad (2.2.26b) \\ n-1 & \text{(HE mode)} \quad (2.2.26c) \end{cases} .$$

In equation (2.2.25), the modes with the common parameter m, 1 have the same eigenvalues (strictly different but approximate). This is the dispersion equation of the core mode.

Since the dispersion equation of the clad mode is very complicate and difficult to explain in details, for the sake of the simplicity, here we just give the results below, which can be expressed by

$$\zeta_0 = \zeta_1. \quad (2.2.27)$$

But here

$$\zeta_0 = \frac{1}{\sigma_2} \frac{u_2 \left(JK + \frac{\sigma_1 \sigma_2 u_{21} u_{32}}{{n_2}^2 a_1 a_2} \right) p_l(a_2) - K q_l(a_2) + J r_l(a_2) - \frac{1}{u_2} s_l(a_2)}{-u_2 \left(\frac{u_{32}}{{n_2}^2 a_2} J - \frac{u_{21}}{{n_1}^2 a_1} K \right) p_l(a_2) + \frac{u_{32}}{{n_1}^2 a_2} q_l(a_2) + \frac{u_{32}}{{n_2}^2 a_2} r_l(a_2)}$$

$$\zeta_1 = \sigma_1 \frac{u_2 \left(\frac{u_{32}}{a_2} J - \frac{{n_3}^2 u_{21}}{{n_2}^2 a_1} K \right) p_l(a_2) - \frac{u_{32}}{a_2} q_l(a_2) - \frac{u_{21}}{a_1} r_l(a_2)}{u_2 \left(\frac{{n_3}^2}{{n_2}^2} JK + \frac{\sigma_1 \sigma_2 u_{21} u_{32}}{{n_1}^2 a_1 a_2} \right) p_l(a_2) - \frac{{n_3}^2}{{n_1}^2} K q_l(a_2) + J r_l(a_2) - \frac{{n_2}^2}{{n_1}^2 u_2} s_l(a_2)},$$

and here the following parameters are assumed.

$$\sigma_1 = i \frac{l n_{eff}}{Z_0}$$

$$\sigma_2 = i \, l n_{eff} Z_0$$

$$u_{21} = \frac{1}{u_2{}^2} - \frac{1}{u_1{}^2}$$

$$u_{32} = \frac{1}{w_2{}^2} - \frac{1}{w_1{}^2}$$

$$u_j{}^2 \equiv \left(\frac{2\pi}{\lambda}\right)^2 \left(n_j{}^2 - n_{eff}{}^2\right) \quad [j \in 1,2]$$

$$w_3{}^2 \equiv \left(\frac{2\pi}{\lambda}\right)^2 \left(n_{eff}{}^2 - n_3{}^2\right)$$

$$J \equiv \frac{J_l{}'(u_1 a_1)}{u_1 J_l(u_1 a_1)}$$

$$K \equiv \frac{K_l{}'(u_1 a_1)}{w_3 K_l(w_3 a_2)}$$

$$p_l(r) \equiv J_l(u_2 r)N_l(u_2 a_1) - J_l(u_2 a_1)N_l(u_2 r)$$

$$q_l(r) \equiv J_l(u_2 r)N_l{}'(u_2 a_1) - J_l{}'(u_2 a_1)N_l(u_2 r)$$

$$r_l(r) \equiv J_l{}'(u_2 r)N_l(u_2 a_1) - J_l(u_2 a_1)N_l{}'(u_2 r)$$

$$p_l(r) \equiv J_l{}'(u_2 r)N_l{}'(u_2 a_1) - J_l{}'(u_2 a_1)N_l{}'(u_2 r)$$

Eq. (2.2.7) is the so-called dispersion equations for the cladding modes. To numerically solve this equation, the effective refractive index n_{eff}^{cl} of the cladding mode and thus the clad mode distribution can numerically be obtained.

3. Basic theory of the long-period fiber grating

3.1 Definition of the long-period fiber grating (LPG)

The fiber grating is produced by making an optical fiber with axial periodic refractive index-change. Generally, for simplicity we assume that a perturbation to the effective refractive index n_{eff} of the guided modes is of our interest [1], which can be described by

$$\delta n_{eff}(z) = \overline{\delta n}_{eff}(z)\left\{1 + v\cos\left[\frac{2\pi}{\Lambda}z + \phi(z)\right]\right\}, \tag{3.1.1}$$

where $\overline{\delta n_{eff}}(z)$ is the direct current index change spatially averaged over a grating period, v is the fringe visibility of the index change, Λ is the period of fiber grating, and $\phi(z)$ describes grating chirp.

According to the coupling characteristic of the existed modes in fiber grating, we can divide the fiber grating into two types: fiber Bragg grating (FBG) and long period fiber grating (LPG). The long period fiber grating (LPG) where the forward core-mode is coupled to the forward cladding modes, has representative period of several hundred micrometers. As shown in Fig. 3.1, the LPG could functions as a broadband band-rejection filter in transmission spectrum, therefore it is also called the transmission grating. Basing on the phase-matching conditions, the resonant wavelength λ_L shown in Fig. 3.1.1 can be expressed as

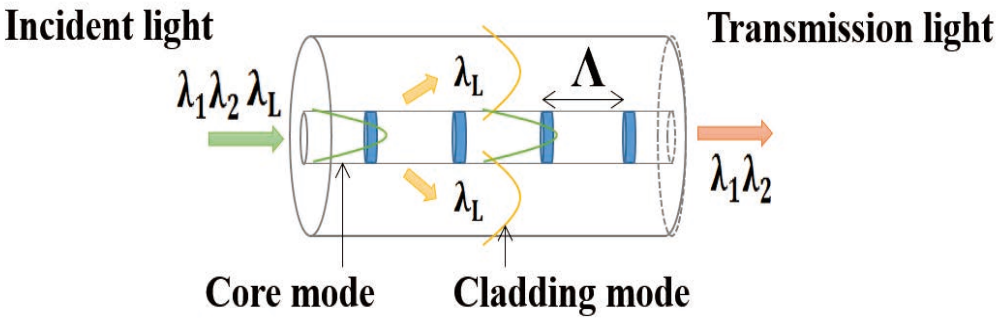

Fig. 3.1.1. The structure mode of long period fiber grating

$$\lambda_L = \left(n_{eff}^{co} - n_{eff}^{cl}\right)\Lambda, \tag{3.1.2}$$

Where Λ is the period of LPG, and the n_{eff}^{co} and n_{eff}^{cl} are the effective refractive index of the core- and the cladding-mode, respectively.

3.2 The coupled mode theory

We assume that the horizontal part of the electric field E_t can be written as the superposition of the eigenmodes, and make use j to mark the j_{th} eigenmode [1]:

$$E_t(x,y,z,t) = \sum_j \left[A_j(z)\exp(i\beta_j z) + B_j(z)\exp(i\beta_j z)\right]\vec{e}_{jt}(x,y)\exp(-i\omega t), \tag{3.2.1}$$

where the $A_j(z)$ and $B_j(z)$ represent the forward and backward transmission amplitude along the z axis of j order mode, respectively. And the $e_{jt}(x,y)$ represents the transverse mode field component of j_{th} order mode, it can represent not only the cladding mode but also the radiation mode. The β_j represents the propagation constant of j_{th} order mode.

In fiber grating, the effective refractive index of mode can be expressed by

$$\delta n_{eff}(z) = \overline{\delta n}_{eff}(z)\left\{1 + v\cos\left[\frac{2\pi z}{\Lambda} + \phi(z)\right]\right\}, \tag{3.2.2}$$

where the $\overline{\delta n}_{eff}(z)$ express the "dc" index-change of fiber grating; v is the fringe visibility of refractive index modulation; Λ is the period of fiber grating; $\phi(z)$ represents the chirp of fiber grating. The periodical index-modulation can make the different modes existed in the fiber coupled with each other, particularly, the amplitude change of the j_{th} mode along the z axis can be expressed as [1]

$$\frac{dA_j}{dz} = i\sum_k A_k\left(\kappa_{kj}^t + \kappa_{kj}^z\right)\exp\left[i\left(\beta_k - \beta_j\right)z\right] + i\sum_k B_k\left(\kappa_{kj}^t - \kappa_{kj}^z\right)\exp\left[-i\left(\beta_k + \beta_j\right)z\right] \tag{3.2.3}$$

$$\frac{dB_j}{dz} = -i\sum_k A_k\left(\kappa_{kj}^t - \kappa_{kj}^z\right)\exp\left[i\left(\beta_k + \beta_j\right)z\right] - i\sum_k B_k\left(\kappa_{kj}^t + \kappa_{kj}^z\right)\exp\left[-i\left(\beta_k - \beta_j\right)z\right] \tag{3.2.4}$$

The β_k is the propagating constant of k order mode; κ_{kj}^t is the transverse mode coupling coefficient of k_{th} order mode.

$$\kappa_{kj}^t(z) = \frac{\omega}{4}\iint_{\sim} dxdy\Delta\varepsilon(x,y,z)e_{kt}(x,y)e_{jt}^*(x,y), \tag{3.2.5}$$

where $\Delta\varepsilon$ is the perturbation of dielectric, when $\delta n \ll n$ $\Delta\varepsilon \approx 2n\delta n$; e_{kt} is the transverse mode field component; the "*" represent the complex conjugate; in Eq. (3.2.4) and Eq. (3.2.5), longitudinal mode coupling coefficient $\kappa_{kj}^t(z)$ and $\kappa_{kj}^z(z)$ of the j_{th} mode and k_{th} mode have similar expression, but since $\kappa_{kj}^z(z)$ is much less than $\kappa_{kj}^t(z)$, it can be ignored. The Eq. (3.2.5) is very important, it reveals that the refractive index perturbation is the origin which causes the mode coupling between the eigenmodes.

The effective refractive index-change of the core $\delta n_{co}(z)$ can also be expressed by Eq. (3.2.2) but only replacing the $\bar{n}_{eff}(z)$ with $\bar{n}_{co}(z)$. For fiber grating in which the index-modulation mainly lies in the core, we have two new parameters below

$$\sigma_{kj}(z) = \frac{\omega n_{co}}{2}\overline{\delta n}_{co}(z)\iint_{core} dxdye_{kt}(x,y)e_{jt}^*(x,y) \tag{3.2.6}$$

$$\kappa_{kj}(z) = \frac{v}{2}\sigma_{kj}(z). \tag{3.2.7}$$

Among these equations, $\sigma_{kj}(z)$ is the "dc" coupling coefficient; $\kappa_{kj}(z)$ is the "ac" coupling coefficient. So the transverse coupling coefficient in Eq. (3.2.5) can simply be

expressed by

$$\kappa_{kj}^{t}(z) = \sigma_{kj}(z) + 2\kappa_{kj}(z)\cos\left[\frac{2\pi z}{\Lambda} + \phi(z)\right]. \tag{3.2.8}$$

The mode couplings happened in a LPG main occur between the fundamental core mode (LP_{01}) and the cladding modes. In general, there exist many cladding modes in the LPG, therefore in the transmission spectrum of the LPG, there exist several loss peaks in the spectral region of several hundred nanometers. These loss peaks are mutual independence, and for most of the cases, only one loss peak is of our interest, so through our study below, we only consider the couplings between the core-mode with one particularly cladding mode.

We assume that the required resonance wavelength of LPG is λ_D, which can be determined by

$$\lambda_D \equiv \left(n_{eff}^{co} - n_{eff}^{cl}\right)\Lambda = \Delta n_{eff}\Lambda, \tag{3.2.9}$$

where n_{eff}^{co} and n_{eff}^{cl} are the effective refractive index of LP_{01} core mode and one of the cladding modes, respectively. Eq. (3.2.9) is obtained from the phase matching condition of LPG. The wave-number detuning is

$$\delta \equiv \frac{1}{2}(\beta_{co} - \beta_{cl}) - \frac{\pi}{\Lambda} = \pi\Delta n_{eff}\left(\frac{1}{\lambda} - \frac{1}{\lambda_D}\right), \tag{3.2.10}$$

where β_{co} and β_{cl} are the propagating constants of the LP_{01} core mode and one typical cladding mode, respectively. We further define the "dc" self-coupled coefficient $\hat{\sigma}$ as

$$\hat{\sigma} \equiv \delta + \frac{\sigma_{11} - \sigma_{22}}{2} - \frac{1}{2}\frac{d\phi}{dz}, \tag{3.2.11}$$

where the σ_{11} and σ_{22} are the "dc" coupling coefficient which are defined by Eq. (3.2.6). Through the synchronous approximation, the Eq. (3.2.3) and Eq. (3.2.4) can be rewritten as:

$$\frac{dR}{dz} = i\hat{\sigma}R(z) + i\kappa S(z), \tag{3.2.12}$$

$$\frac{dS}{dz} = -i\hat{\sigma}S(z) + i\kappa^* R(z), \tag{3.2.13}$$

among these two equations, κ is the "ac" coupling coefficient. R and S are the amplitude of core and cladding, respectively, define by

$$R(z) \equiv A_1 \exp\left[-\frac{i(\sigma_{11}+\sigma_{22})z}{2}\right] \exp\left(i\delta z - \phi/2\right) \tag{3.2.14}$$

$$S(z) \equiv A_2 \exp\left[-\frac{i(\sigma_{11}+\sigma_{22})z}{2}\right] \exp\left(-i\delta z - \frac{\phi}{2}\right). \tag{3.2.15}$$

In the following, we numerically investigate the transmission spectrum of LPG. Boundary conditions of the LPG with length of L are assumed to be $R(0) = 1$ and $S(0) = 0$. For uniform LPG, $\overline{\delta n_{eff}}$ is a constant and $\frac{d\phi}{dz} = 0$, so that $\hat{\sigma}$ and κ are constant. The Eq. (3.2.14) and (3.2.15) are the first order differential equation with constant coefficient. The self-coupled rate $t_=$ and cross-coupled rate $t_\times$ are expressed as

$$t_= = \frac{|R(z)|^2}{|R(0)|^2} = \cos^2\left(\sqrt{\kappa^2+\hat{\sigma}^2}z\right) + \frac{1}{1+\kappa^2/\hat{\sigma}^2}\sin^2\left(\sqrt{\kappa^2+\hat{\sigma}^2}z\right) \tag{3.2.16}$$

$$t_\times = \frac{|S(z)|^2}{|S(0)|^2} = \frac{1}{1+\hat{\sigma}^2/\kappa^2}\sin^2\left(\sqrt{\kappa^2+\hat{\sigma}^2}z\right). \tag{3.2.17}$$

When we simulate the transmission spectrum of LPG, we usually calculate the $t_{=}$ from core mode, because of we just can observe the transmission spectrum of core mode in OSA. From the expression of $t_{\times}$, when $\hat{\sigma} = 0$, the cross-coupled rate, which is generally called the transmission of LPG becomes the maximum

$$t_{\times,max} = \sin^2(\kappa L). \tag{3.2.18}$$

To substitute $\hat{\sigma} = 0$ into the Eq. (3.2.11) and combine it with the Eq. (3.2.10), we can get the real resonance wavelength of LPG as:

$$\lambda_{res} = \frac{1}{1 - (\sigma_{11} - \sigma_{22})\frac{\Lambda}{2\pi}}\lambda_D. \tag{3.2.19}$$

Since the index-modulation mainly occurs in the core and index-modulation in the cladding is very small, the condition of $\sigma_{11} \ll \sigma_{22}$ is satisfied, so σ_{11} can be simply expressed as

$$\sigma_{11} = \sigma = \frac{2\pi}{\lambda}\overline{\delta n}_{eff}. \tag{3.2.20}$$

Eq. (3.2.19) then can be approximately expressed by

$$\lambda_{res} \approx \left(1 + \frac{\overline{\delta n}_{eff}}{\Delta n_{eff}}\right)\lambda_D. \tag{3.2.21}$$

The above equation shows that due to the existence of the DC part of the index-modulation, the real loss peak of LPG is not at the design wavelength λ_D. The offset is determined by the $\overline{\delta n}_{eff}$, which is dependent on the LPG writing method and the gating mechanism.

For uniform LPG with the index-modulation visibility $\nu = 1$ is assumed, then from the Eqs. (3.2.10), (3.2.11) and (3.2.20), we can get the dc self-coupled coefficient $\hat{\sigma}$ by

$$\hat{\sigma} = \pi\left[\frac{\Delta n_{eff} + \overline{\delta n}_{eff}}{\lambda} - \frac{1}{\Lambda}\right]. \tag{3.2.22}$$

From Eq. (3.2.8) and Eq. (3.2.20), the cross-coupled coefficient κ of uniform LPG can simply be expressed by

$$\kappa = \pi\overline{\delta n}_{eff}/\lambda. \tag{3.2.23}$$

Here we define the bandwidth $\Delta\lambda$ as the spacing between λ_1 and λ_2 which are the first zero-value point ($t_\times = 0$) on both sides of the transmission loss peak. From equation (3.2.17), when $t_\times = 0$,

$$(\kappa^2 + \hat{\sigma}^2)L^2 = \pi^2. \tag{3.2.24}$$

Substitute the Eqs. (3.2.22) and (3.2.23) into the Eq. (3.2.24), we can get a quadratic equation with one unknow. The difference of the equation`s two roots is the bandwidth $\Delta\lambda$ of LPG when non-coupling occur (no power of cladding mode coupling back to core mode)

$$\Delta\lambda = |\lambda_2 - \lambda_1| = 2\sqrt{\frac{\left(\lambda_D + \Lambda\overline{\delta n}_{eff}\right)^2}{N^2} - \Lambda^2\overline{\delta n}_{eff}^{\,2}}. \tag{3.2.25}$$

In the above equation, N is the period number of LPG, so $N = \Lambda * L$ and $N \gg 1$ is generally satisfied. For weekly coupled LPG with small refractive index modulation, we can ignore the factor of $\overline{\delta n}_{eff}$, so the $\Delta\lambda$ can simply be expressed

$$\Delta\lambda \approx \frac{2\lambda_D}{N}. \tag{3.2.26}$$

The above equation shows that in the same refractive index modulation, the spectral bandwidth of the LPG is inversely proportional to the number of period or the length of grating, which is correct even for the gratings with a large refractive index-modulation.

Figure 3.2.1 show the simulation result for transmission spectrum of a uniform LPG, where the grating's parameters are adopted as the follows: $\Delta n_{eff} = 2.6 \times 10^{-3}$, $\overline{\delta n}_{eff} = -2.5 \times 10^{-5}$, the grating period $\Lambda = 640$, the grating number is N = 50 and N = 55, respectively. From this figure, we can find that with the increment of the grating number, the bandwidth of transmission spectrum decrease, which is exactly the same as what we expect in Eq. (3.2.26).

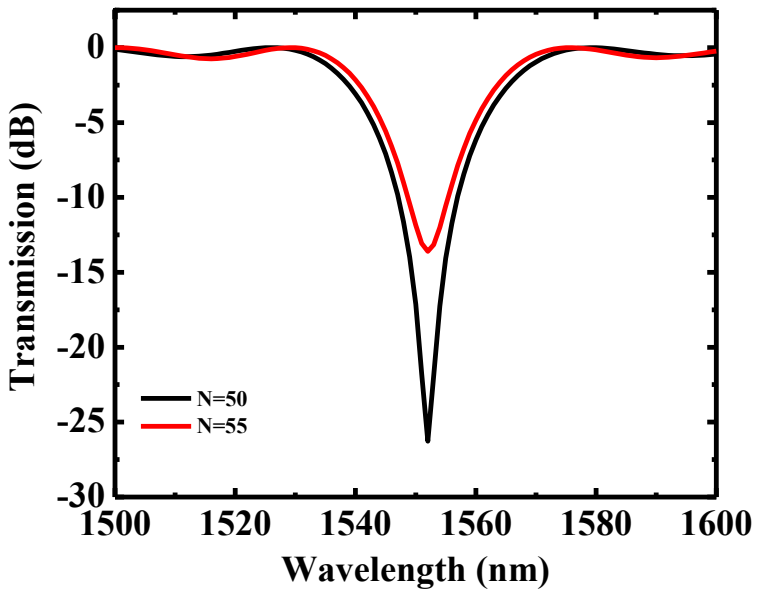

Fig 3.2.1. The transmission spectra with different grating number

3.3 Transfer matrix method

To date, the numerical means: transfer matrix method (TFM) has generally been used to analyze the fiber gratings, especially for a non-uniform LPG [1]. In principle for any one non-uniform grating, it can be divided as many uniform sections and each of which has a constant period. The details procedures are introduced as follows. Firstly, a single uniform grating with a length of Δz and period of Λ is considered. We can define R_i and S_i as the field amplitudes after transmitting the section i. If only the two modes coupling are only considered, the coupling equations described above have an analytical solution, which can be expressed in a matrix form like

$$\begin{bmatrix} R_i \\ S_i \end{bmatrix} = \mathbf{F}_i \cdot \begin{bmatrix} R_{i-1} \\ S_{i-1} \end{bmatrix}, \tag{3.3.1}$$

where $\mathbf{F_i}$ represents the propagating 2x2 matrix which have four elements and can be expressed

$$T_{11} = \cos(\gamma \Delta z) + i\frac{\hat{\sigma}}{\gamma}\sin(\gamma \Delta z) \tag{3.3.2}$$

$$T_{12} = i\frac{\kappa}{\gamma}\sin(\gamma \Delta z) \tag{3.3.3}$$

$$T_{21} = i\frac{\kappa}{\gamma}\sin(\gamma \Delta z) \tag{3.3.4}$$

$$T_{22} = \cos(\gamma \Delta z) - i\frac{\hat{\sigma}}{\gamma}\sin(\gamma \Delta z), \tag{3.3.5}$$

where

$$\gamma = \sqrt{\kappa^2 + \hat{\sigma}^2}, \tag{3.3.6}$$

and $\hat{\sigma}$, and κ are defined in the preceding section. If the matrices for all the individual sections are known, one can obtain the output amplitudes from the following equation:

$$\begin{bmatrix} R_M \\ S_M \end{bmatrix} = \mathbf{F} \begin{bmatrix} R_0 \\ S_0 \end{bmatrix}; \mathbf{F} = \mathbf{F_M} \cdot \mathbf{F_{M-1}} \cdot \ldots \cdot \mathbf{F_i} \cdot \ldots \cdot \mathbf{F_1}. \tag{3.3.7}$$

The number of sections M is determined by the required accuracy. M may not be made arbitrarily large. In general, $\Delta z \gg \Lambda$ is required and which means that one must maintain

$$M \ll \frac{2n_{eff}L}{\lambda_D}. \tag{3.3.8}$$

The transmission coefficient t of LPG is expressed by

$$t = \frac{R(-L/2)}{R(L/2)} = T_{11} = \cos(\gamma \Delta z) + i\frac{\hat{\sigma}}{\gamma}\sin(\gamma \Delta z). \tag{3.3.9}$$

The power transmission is then

$$T = |t|^2 = \cos^2(\gamma \Delta z) + \frac{\hat{\sigma}^2}{\gamma^2}\sin^2(\gamma \Delta z). \tag{3.3.10}$$

Especially for $\hat{\sigma} = 0$, T has the minimum value

$$T_{min} = \cos^2(\gamma \Delta z). \tag{3.3.11}$$

3.4 The phase-shifted LPG and the cascaded LPGs

In the past few decades, study on the phase-shifted LPG and cascaded LPG have attracted a lot of research interests. To date, the phase-shifted LPG has generally been used as a band-pass filter or sensing component. Structure of them is shown like the one in Fig. 3.4.1.

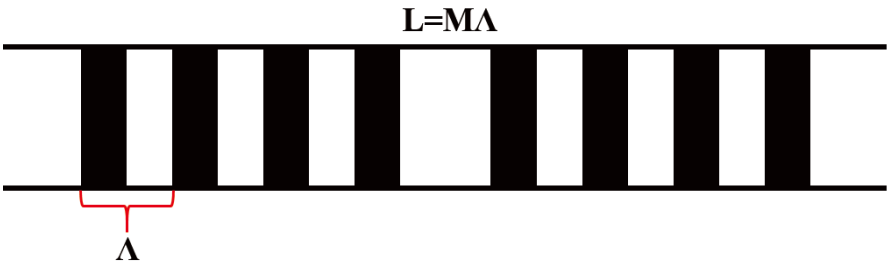

Fig. 3.4.1. The structure of phase-shift LPG

Fig. 3.4.1 shows a uniform LPG with N periods, which can be simply regarded as two gratings, LPG1 and LPG2, but separated by a phase shift ϕ and a length of fiber d. when $\phi = 0$ and d=0, it becomes a conventional LPG, when d=0 and $\phi \neq 0$, we call it phase-shifted LPG and when $d \gg \Lambda$, we call it cascaded LPG. Considering the boundary conditions $A_1(0) = 1$, $A_2(0) = 0$, the output amplitude is written as [3]

$$\begin{bmatrix} R_M \\ S_M \end{bmatrix} = \begin{bmatrix} R_2 \\ S_2 \end{bmatrix} \begin{bmatrix} e^{j\pi(n_{co}-n_{cl})d/\lambda} & 0 \\ 0 & e^{-j\pi(n_{co}-n_{cl})d/\lambda} \end{bmatrix} \times \begin{bmatrix} e^{j\phi/2} & 0 \\ 0 & -e^{j\phi/2} \end{bmatrix} \begin{bmatrix} R_1 \\ S_1 \end{bmatrix} \begin{bmatrix} 1 \\ 0 \end{bmatrix}, \tag{3.3.12}$$

where n_{co} and n_{cl} are refractive indices of the core mode and cladding mode, respectively. Figure 3.4.2 shows simulation results of the transmission spectra. In this figure, three different phase shifts (0π, $\pi/2$, π, $3\pi/2$) were inserted at the middle of fiber.

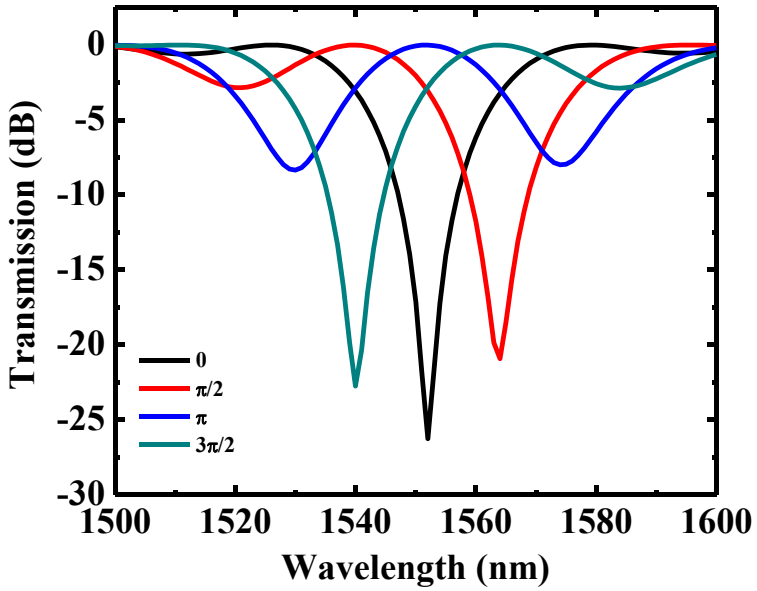

Fig. 3.4.2. Simulation result of transmission spectra with three different phase shifts

For cascaded LPG, the structure is shown as in Fig. (3.4.3), where the light is split into two, the phase delay between the two arms is wavelength dependent and as a result, the transmission spectrum is modulated with multiple peaks. This kind of devices is similar to a Mach-Zehnder interferometer. For the light propagating through the two LPGs, the relative phase difference between core mode and cladding mode can be expressed as [4]

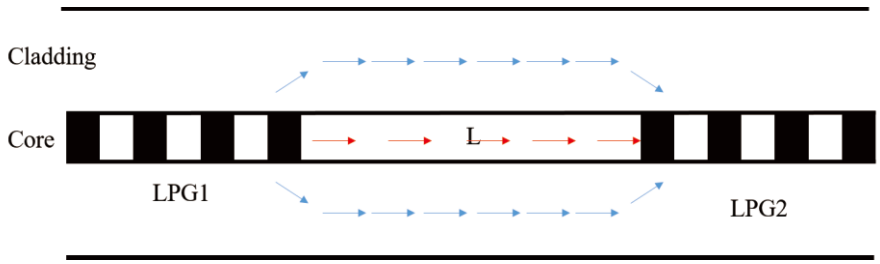

Fig. 3.4.3. Structure of the cascaded LPG

$$\Psi = \Phi_{in}(\lambda, d) - [\beta_{out}^{co}(\lambda) - \beta_{out}^{cl}(\lambda)](L - d), \qquad (3.3.13)$$

where d is the length of every grating; L is the length between the two grating; $\beta_{out}^{co}(\lambda)$ and $\beta_{out}^{cl}(\lambda)$ are the propagating constants of core mode and cladding mode in non-grating region, respectively; and the $\Phi_{in}(\lambda, d)$ is the total phase shift of core mode and cladding mode. Base on principle of interference, if $\phi = 2N\pi$ (N is integer), we can get the interference peaks. The spacing of adjacent interference peaks can be found by

$$\Delta\lambda = \frac{2\pi}{\frac{d}{d\lambda}\Phi_{in}(\lambda, d) - \frac{d}{d\lambda}[\beta_{out}^{co}(\lambda) - \beta_{out}^{cl}(\lambda)](L - d)}. \quad (3.3.14)$$

Because the refractive indices are changed by introduced by LPG, the average refractive index in grating region and refractive index in non-grating region are different. So the total phase shift of two LPGs can be approximately expressed as

$$\Phi_{in} = -\left[\beta_{in}^{co}(\lambda) - \beta_{in}^{cl}(\lambda)\right]d, \quad (3.3.15)$$

where $\beta_{in}^{co}(\lambda)$ and $\beta_{in}^{cl}(\lambda)$ are the propagating constant of core mode and cladding mode in grating region, respectively. To substitute the equation (3.3.15) into equation (3.3.14), and makes use the definition of propagating constant

$$\beta = \frac{2\pi n_{eff}}{\lambda}. \quad (3.3.16)$$

Where n_{eff} is the effective refractive index, so $\Delta\lambda$ can be expressed as

$$\Delta\lambda = \frac{\lambda^2}{\Delta S_{in} d + \Delta S_{out}(L - d)}, \quad (3.3.17)$$

where ΔS_{in} and ΔS_{out} are the effective refractive index of grating region and non-grating

region. And the ΔS_{in} and ΔS_{out} can be expressed as

$$\Delta S_{in,out} = \Delta n_{eff} - \lambda \frac{d}{d\lambda} \Delta n_{eff}, \tag{3.3.18}$$

where Δn_{eff} is the difference between core mode and cladding mode. When the L is much larger than the d, $\Delta S_{in} \approx \Delta S_{out}$, the $\Delta\lambda$ can be approximately expressed as

$$\Delta\lambda = \frac{\lambda^2}{\left(\Delta n_{eff} - \lambda \frac{d}{d\lambda} \Delta n_{eff}\right) L} = \frac{\lambda^2}{\Delta S_{out} L}. \tag{3.3.19}$$

In the above equation, the additional term $\frac{d}{d\lambda}\Delta n_{eff}$ is included, which is general called the dispersion factor. If this term (the dispersion effect) can be neglected, then the Eq. (3.3.19) can be further simplified as

$$\Delta\lambda \approx \frac{\lambda^2}{\Delta n_{eff} L}. \tag{3.3.20}$$

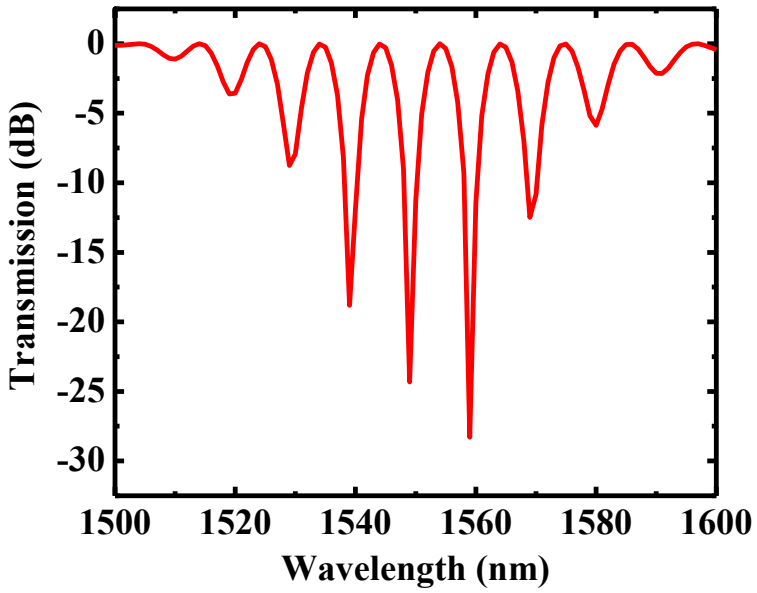

Fig. 3.4.4. Simulation result of the cascaded two LPGs with spacing d = 80mm

Figure 3.4.4 shows the simulation results of cascaded two same LPGs, where the two grating are identical and the spacing of them 80 mm. Form this figure, one can obviously see that the original peak is split into multiple ones and each has a constant spacing to the neighbor ones in spectrum.

References

[1]. T. Erdogan," Fiber grating spectra," IEEE J. Lightwave Technol., 15(8) 1277-1294 (1997)

[2]. A. Yariv," Coupled-mode theory for guided-wave optics," IEEE J. Quantum Electron., QE-9 919-933 (1973)

[3]. Y. Liu, J.A.R. Williams, L. Zhang and I. Bennion, "Phase shifted and cascaded long-period fiber gratings," Opt. Commun. 164, 27-31 (1999)

4. Fabrication of phase-shifted long period fiber grating and its application to strain measurement

4.1 Introduction

In the past few decades, phase-shifted long-period fiber grating (LPG) has been widely studied and have found various applications in the fields of optical communications, all-optical signal processing, and optical fiber sensors etc. [1]–[7]. To date, various methods have been developed to produce a phase shift in a common LPG. In generally the phase shift can be permanently inserted into a fiber grating by using either the UV post-processing [8], or the post-writing and -etching techniques [6], [7]. However, all the above methods need either an expensive UV writing system or otherwise a very complicate and time-consuming etching and coating procedures. Recently, a simple and cost-efficient technique for fabrication of phase-shifted LPG has been proposed and experimentally demonstrated by Y. Gu et al. [9], which is based on utilization of a computer-controlled CO_2 laser. However the authors there had paid more attentions to realization of the grating's appodization, spectral characteristics of the gratings in terms of the inserted phase-shifts have rarely been experimentally investigated. On the other hand, referring to a phase-shifted LPG, it is generally known that owing to the inserted phase-shift, each of the loss-peaks in transmission spectrum (corresponding to couplings between the forward core mode and different cladding modes) will be split into two and wavelengths of these two peaks are very sensitive to both the ambient temperature and the applied axial strain. Thus, there always exists a need to develop a simple and new technique enabling to discriminate these two effects simultaneously. To date, various approaches have been proposed and demonstrated to address this problem [10]–[16], such as those involving an addition of fiber Bragg grating [10] and an superimposed LPG [11], two LPGs [12], one LPG inscribed on a polarization-maintaining fiber [13], or one LPG but with measuring the wavelength

shifts for two different loss peaks [14], and the combination of a LPG with a high-birefringence fiber loop mirror [15], etc. However, most of the methods proposed above have been accomplished just by adding an additional wavelength-interrogating component. Moreover, due to the weak strain-resistance of the utilized grating, the maximum strain measured is generally limited to a value less than 2000 με, which is still small not enough to cover the total elastic range of the metal structures. In this chapter, firstly several kinds of phase-shifted LPGs have been fabricated and experimentally investigated, where both the grating and the inserted phase-shift are obtained simultaneously by using CO_2 laser. Moreover, by particularly using a π phase-shifted LPG, a robust temperature-insensitive sensor that allows for large strain measurement up to 7600 με is proposed and successfully demonstrated.

4.2 Fabrication and experiment setup

The experimental setup is shown in Fig.4.2.1, which consists of a CO_2 laser controlling system, a beam moving and a focusing system located at a motorized translation stage, a fiber alignment stage, and a measuring system for the transmission spectrum of the LPG, where the utilized fiber is the commonly-used single-mode fiber provided by Fujikura Inc. The CO_2 laser (SYNRAD-20, emission central wavelength of 10.6 μm) works at a high repetition rate of 5 kHz and its duty-cycle is changeable between 1% to 99%. For the grating fabrication, the aligned CO_2 laser beam is focused through a ZnSe lens with a focus length of 70 cm, the minimum spot size on the fiber is ~110 μm, which makes the focusing light mainly absorbed by the fiber within a short period of time, and thus result in a permanent index-change within the exposure region of the fiber core through the thermal shock effect [17].

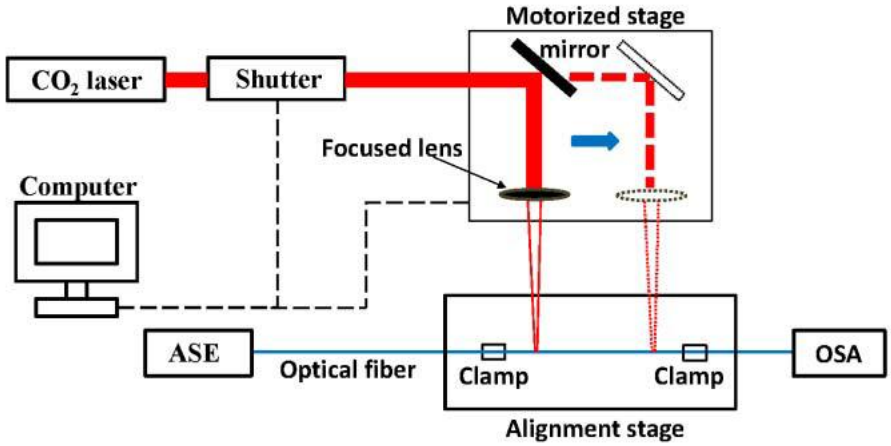

Fig. 4.2.1. Experimental setup for fabrication of phase-shifted LPG

For fabrication of a phase-shifted LPFG, the principle scheme can be arranged as shown in Fig. 4.2.2(a). For comparison, Fig. 4.2.2(b) shows the fabrication scheme of a LPG without phase-shift. Unlike those post-processing methods in which the phase shift is formed after the fabrication of LPFG is completed, here the grating and phase-shift is obtained simultaneously. Moreover, it is seen that any magnitude of the phase-shift Φ could be easily and precisely obtained as long as an additional space of $P = \Phi/(2\pi)\times\Lambda$ is inserted

at local period of the grating where the phase shift is expected to be inserted. In our case, period of the LPG is precisely controlled by periodically turning on/off the laser shutter and meanwhile the motorized translation stage is driven to move forward at a constant speed, as shown in Fig. 4.2.1. The phase shift inserted is obtained just by adding an additional "off" time within particularly period of the shutter. All of the above processes are programmed and realized by using LabView means. For LPG's spectrum measurement, an amplified spontaneous emission (ASE) source and an optical spectral analyzer (OSA) are utilized.

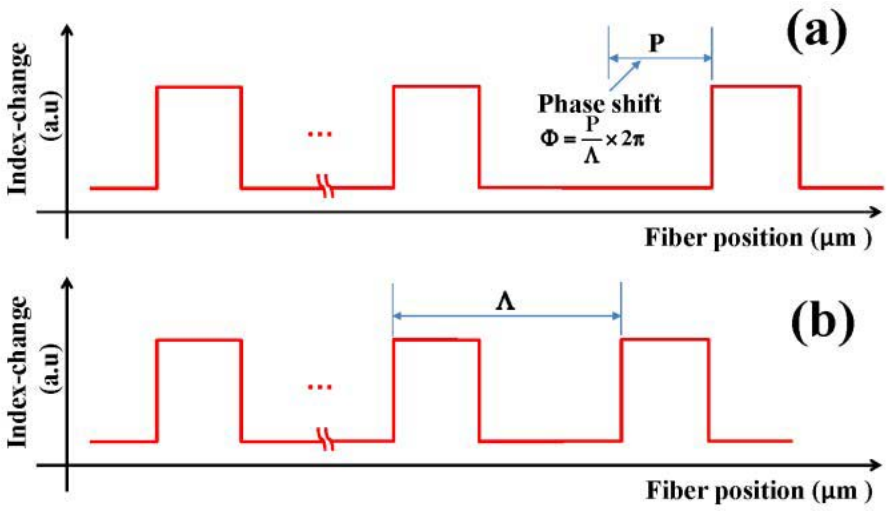

Fig. 4.2.2. Principle scheme for the formation of a phase-shifted LPFG, where an arbitrary phase-shift could be easily and precisely generated (a) Index-change profile with a phase-shift inserted, and (b) without phase-shift inserted.

Three kinds of phase-shifted LPGs with a phase shift of 0, 0.5π, and π, respectively are particularly fabricated, where the grating length and grating pitch are 4 cm and 640 μm, respectively, and all the phase shifts are inserted at middle of the gratings. Figure 3 shows the measured results for these three typical gratings, where Fig. 4.2.3(a), Fig. 4.2.3(b), and Fig. 4.2.3(c) correspond to the gratings with a phase-shift 0, 0.5π, and π, respectively. From this figure, one can easily seen that attributed to the inserted phase shift, the original loss band as shown in Fig.4.2.3(a) is split into two attenuation-band. When the phase shift inserted is less than π, the new resulted band with a larger loss-dip appears on the right side (longer wavelength side) while the other with less loss-dip appears on the left side of the

original LPG's band. Particularly, for π phase shift case as shown in Fig. 4.2.3(c), it can be seen that within the wavelength range of 1530-1570 nm, there exists two nearly symmetrical attenuation bands located at peak wavelength 1536 and 1553 nm, respectively. All the above results agree well with the theoretical calculations obtained in [7] and are surely attributed to the phase-shift inserted into the LPG.

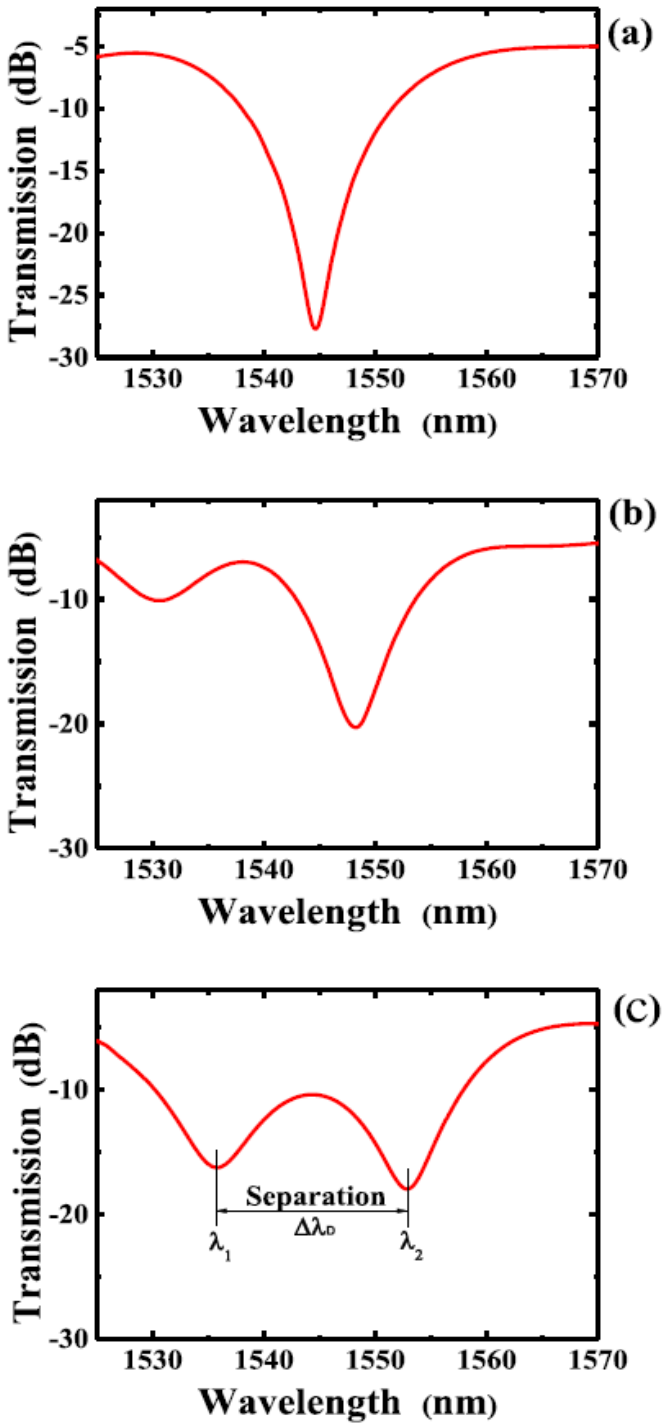

Fig. 4.2.3. Transmission spectra of three phase-shifted LPGs, where the phase shift inserted at middle of the LPG are (a) 0, (b) 0.5 π , and (c) π , respectively.

4.3 Principle and experiment results

As a typical application example of the phase-shifted LPG obtained above, Fig.4.3.1 shows the experimental setup for both the strain and temperature measurements, where the π phase-shifted LPG was utilized and was mounted on two translation stages with epoxy adhesive. The axial strain applied on this LPG was controlled by moving the translation stage on the right-hand side and could be continuously changed within a region of 340-7600 με. Moreover, the LPG was placed in a temperature controller, allowing the temperature to be discretely varied from 20 to 140 °C with a resolution of ±0.1 °C.

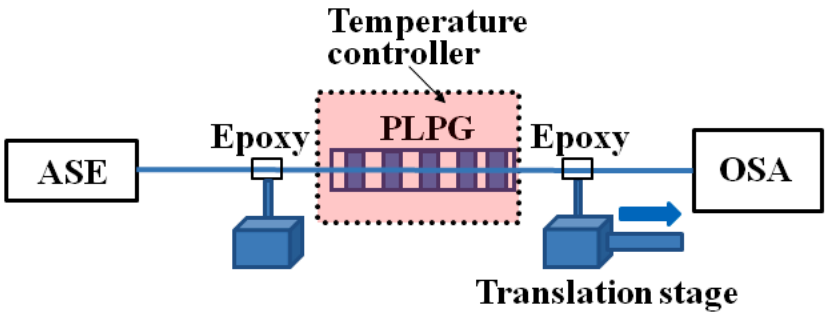

Fig. 4.3.1. Experimental setup for temperature-insensitive strain measurement

For comparison purposes, firstly we measure the transmission spectra of the utilized LPG at seven different temperatures (i.e., 20, 40, 60, 80, 100, 120, and 140 °C) while the strain applied to the LPG is fixed to be 800 με. The measurement for the transmission spectra are shown in Fig. 4.3.2 Fig.4.3.3 shows change of the wavelength separation $\Delta\lambda_D$ (as defined in Fig. 4.2.3) in terms of the temperature.

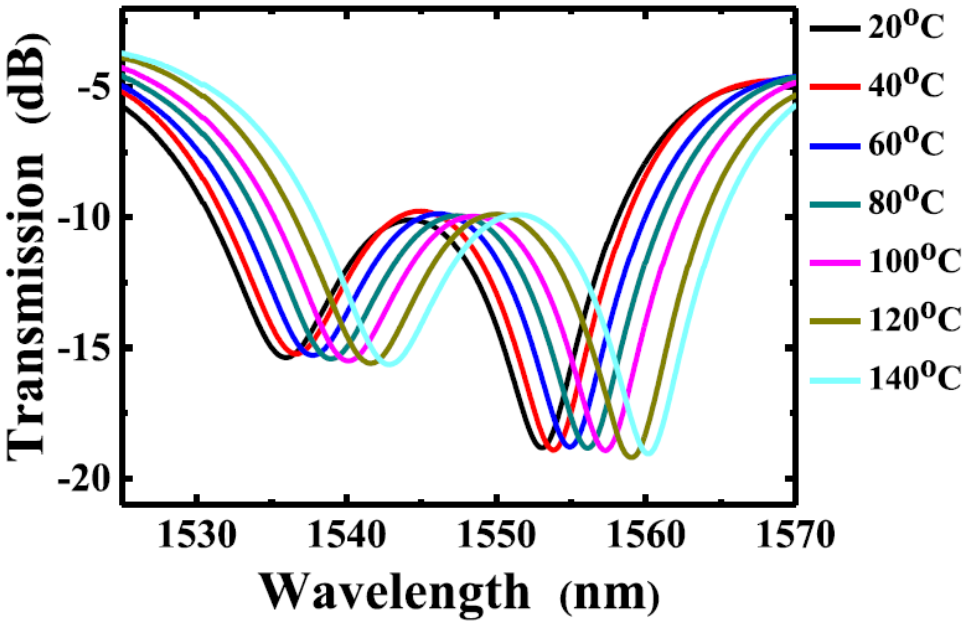

Fig. 4.3.2. Transmission spectra of the phase shifted LPG under different temperatures

From Fig. 4.3.2, it can be seen that as the temperature is increased, the spectrum is linearly shifted to long-wavelength direction with responsivity of ~61 pm/°C, however the separation $\Delta\lambda_D$ is temperature insensitive and almost remain a constant whenever the temperature is changed, which can be obviously found in Fig. 4.3.3.

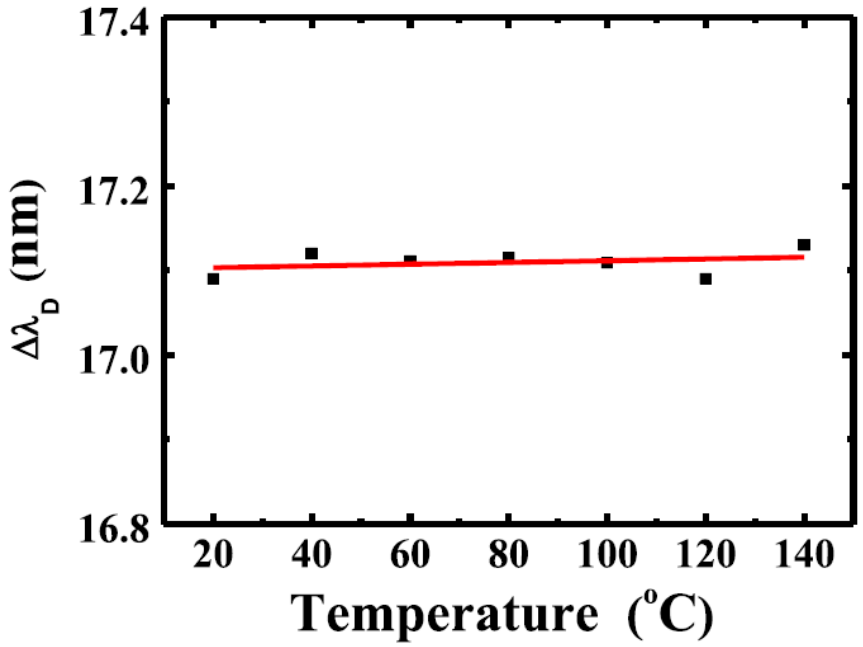

Fig. 4.3.3. Change of the wavelength separation $\Delta\lambda_D$ vs. the temperature at a fixed strain of 800 με

We then measured the transmission spectra of the utilized phase -shifted LPG under several different strains but at a room temperature (24 °C). The results are shown in Fig. 4. 3.4. It is found that as the strain increased, both the attenuation peak are shifted to short wavelength direction, however, they have different strain responses, i.e., the wavelength sensitivity at the left peak is much larger than that of the right peak, which is different from what we know in a general LPG.

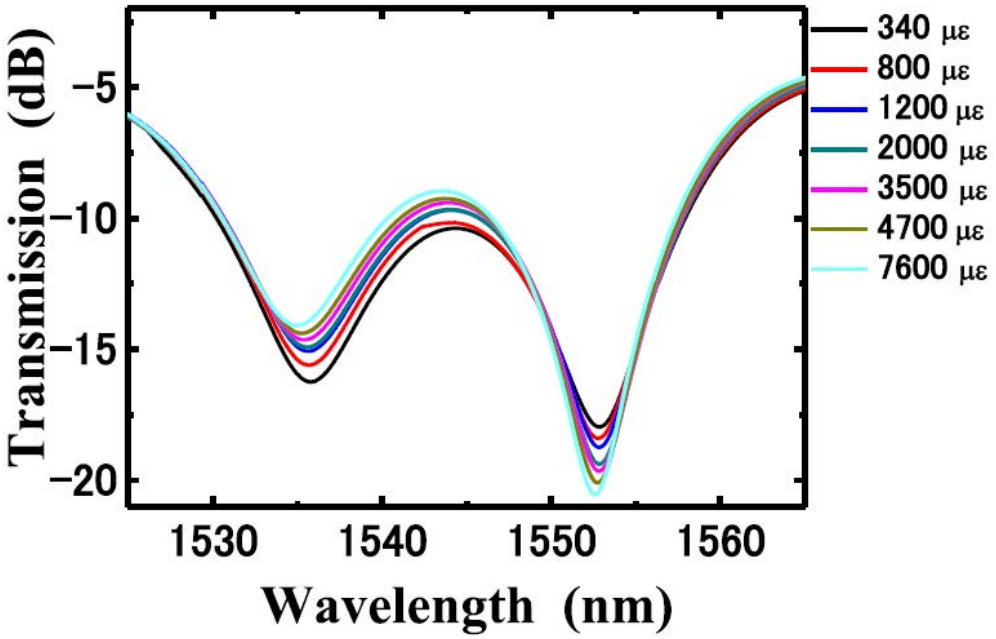

Fig. 4.3.4. Transmission spectrum of the utilized LPG under different strains

As a result of this phenomenon, separation between these two peaks, i.e., $\Delta\lambda_D$ will change in term of the applied strain. Figure 4.3.5 shows measurements and fitting results for the relationship between $\Delta\lambda_D$ and the applied strains. From Fig. 4.3.5, it can be seen that there exists a good one-by-one relationship between the wavelength separation $\Delta\lambda_D$ and the applied strain, and the fitting curve is obtained by using the third-order polynomial evaluation with the result of $R_2 = 0.993$), which can be expressed by

$$\Delta_D(\text{nm}) = 16.9887 + 1.9561 \cdot 10^{-4} \cdot \Delta\varepsilon - 2.386 \cdot 10^{-8} \cdot \Delta\varepsilon^2 + 1.046 \cdot 10^{-12} \cdot \Delta\varepsilon^3 \quad (4.3.1)$$

where the applied strain $\Delta\varepsilon$ is given in a unit of με. Although it is nonlinear equation, compared with the experimental data, it can be found that accuracy of the strain with using Eq. (4.3.1) is estimated to be ±30 με. To verify the accuracy and the temperature cross-effects on the proposed strain sensor, we further investigated the change of the wavelength separation $\Delta\lambda_D$ in terms of the applied strain at temperatures 50 °C and 100 °C,

respectively. The measuring results are shown in Fig. 4.3.5 together.

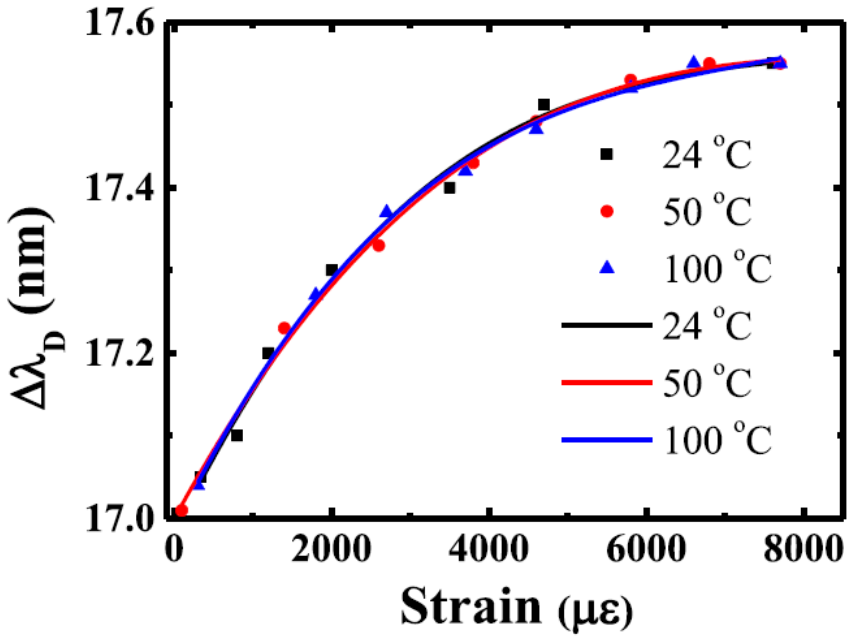

Fig. 4.3.5. Measurement results for the relationship of the wavelength separation $\Delta\lambda_D$ with the applied strain at three different temperatures (24 °C, 50 °C, and 100 °C).

It can be seen that the three fitting curves are well overlapped only with a fractional deviation of 2%, which in return means that the cross-sensitivity between strain and temperature can be neglected even if the temperature and strain are changed simultaneously within the range of 20-140 °C and 300-7600 με, respectively. Moreover, it must be pointed that although the strain sensitivity obtained in our case is very limited, the proposed LPG method allows for a large dynamic strain measurement (300-7600 με), which is nearly 4-time larger than those reported previously [9-15] and may be utilized to measure the strain even for the metal structures.

4.4 Summary

In conclusions, several kinds of phase-shifted LPG are experimentally demonstrated by using the simple and robust CO_2 laser technique, where both the grating and the inserted phase-shift is obtained simultaneously in a single-mode fiber by using CO_2 laser. As an application of this kind of gratings, a novel phase-shifted LPG-based sensor that allows for temperature-insensitive strain measurement has been proposed and successfully demonstrated. The measurement accuracies for the strain were estimated to be ±30 με within the range of 340-7600 με while the temperature is changed in the range of 20-140 °C.

References

[1]. C. D. Pool, C. D. Townsend, and K. T. Nelson, "Helical-grating two-mode fiber spatial-mode coupler," J. Lightwave Technol., vol. 9, no.5, pp. 598–604, May 1991.

[2]. V. I. Kopp, V. M. Churikov, J. Singer, N. Chao, D. Neugroschl, and A. Z. GenacK, "Chiral fiber gratings," Science, vol. 305, no. 5680, pp.74-75, July 2004.

[3]. Ivanov, "Fabrication of long-period fiber gratings by twisting a standard single-mode fiber," Opt. Lett., vol. 30, no. 24, pp. 3290-3292, Dec. 2005.

[4]. S. Oh, K. Lee, U. Paek, and Y. Chung, "Fabricatin of helical long-period fiber gratings by use of a CO_2 laser," Opt. Lett., vol. 29, no. 13, pp. 1464-1466, July 2004.

[5]. W. Shin, B. Yu, Y. Noh, Z. Lee, and D. Ko, "Bandwidth-tunable band-rejection filter based on helicoidal fiber grating pair grating of opposite helicitied," Opt. Lett., vol. 32, no. 10, pp. 1214-1216, May 2007.

[6]. L. Xian, P. Wang, and H. Li, "Power-interrogated and simultaneous measurement of temperature and torsion using paired helical long-period fiber gratings with opposite helicities," Opt. Express, vol. 22, no. 17, pp. 20260-20267, Sept. 2014.

[7]. C. N. Alexeyev, T. A. Fadeyeva, B. P. Lapin, and M. A. Yavorsky, "Generation and conversion of optical vortices in long-period twisted elliptical fibers," Appl. Opt., vol.

51, no.10, pp. C193-C197, Mar. 2012.

[8]. H. Xu and L. Yang, “Conversion of orbital angular momentum of light in chiral fiber gratings,” Opt. Lett., vol. 38, no. 11, pp. 1978-1980, June 2013.

[9]. Y. Rao, Y. Wang, Z. Ran, and T. Zhu, “Novel fiber-optic sensors based on long-period fiber gratings written by high-frequency CO_2 laser pulses,” J. Lightwave Technol., vol. 21, no. 5, pp. 1320-1327, May 2003.

[10]. H. J. Patrick, A. D. Kersey, and F. Bucholtz, “Analysis of the response of long period fiber gratings to external index of refraction,” J. Lightwave Technol., vol. 16, no. 9, pp. 1606-1612, Sept. 1998.

[11]. V. Bhatia, “Applications of long-period gratings to single and multi-parameter sensing,” Opt. Express, vol. 4, no., pp. 457-466, 1999.

[12]. S. W. James and R. P. Tatam, “Optical fibre long-period grating sensors: characteristics and application,” Meas. Sci. Technol., vol. 14, no. 5, pp. R49-R61, May 2003.

[13]. D. Villar, F. Arregui, I. Matias, A. Cusano, D. Paladino, and A. Cutolo, “Fringe generation with non-uniformly coated long-period fiber gratings,” Opt. Express, vol. 15, no. 15, pp. 9326-9340, Aug. 2007.

[14]. Y. Wang, “Review of long period fiber gratings written by CO_2 laser,” J. Appl. Physics, vol. 108, no. 8, pp. 081101-1-081101-18, Oct. 2010.

[15]. H. Xuan, W. Jin, and M. Zhang, “CO_2 laser induced long period gratings in optical microfibers,” Opt. Express, vol. 17, no. 24, pp. 21882-21890, Dec. 2009.

[16]. M. Sumetsky, Y. Dulashko, and A. Hale, “Fabrication and study of bent and coiled free silica nanowires: Self-coupling microloop optical interferometer,” Opt. Express, vol. 12, no. 15, pp. 3521-3531, July 2004.

[17]. T. Erdogan, “Cladding-mode resonances in short- and long-period fiber gratings filters,” J. Opt. Soc. Am. A, vol. 14, no. 8, pp. 1760-1773, Aug. 1997.

5. Helical-type LPG

5.1 Introduction

In the above chapter, we have talked about the conventional and the phase-shifted LPGs which are fabricated by using the point-to-point direct-writing method with the CO_2 laser. Although this method has some of the unique advantages, e. q., the extreme low-cost in term of both the writing and controlling system; much more flexibilities for the fiber selection (suitable for almost any kinds of fiber), and higher temperature stability (can stand high temperature up to 800 ^{o}C) for the fabricated LPG. However, it has some critical disadvantages, such as the high polarization loss, and the extremely low resistant ability to stand for the bending, stretching, pressure, or strain due to the surface defects of the LPG which are inevitably avoided by using the focused CO_2 laser beam technique. In this chapter, we will propose and demonstrate an advanced LPG: a helical-type long period fiber grating (HLPG) which is also fabricated by using a CO_2 laser irradiation method but combined with a sapphire tube technique. To date, mainly two methods to fabricate the HLPG have been proposed and demonstrated, which includes the ones by homogeneously twisting a fiber with a noncircular core cross section [1, 2] and standard single-mode fiber [3] as shown in Fig. 5.1.1, and the others by creating a helical surface deformation along the fiber [4, 5] as shown in Fig. 5.1.2.

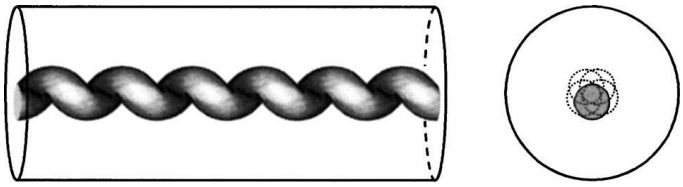

Fig. 5.1.1. Homogeneously twisting a fiber with a noncircular core cross-section (OPTICS LETTERS / Vol. 29, No. 13, 2004)

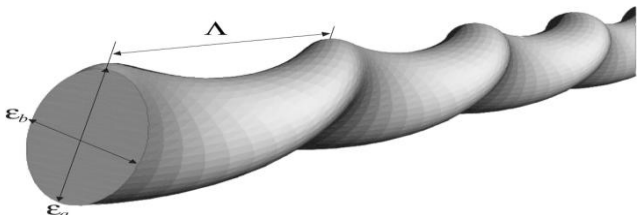

Fig. 5.1.2. Create a helical surface deformation along the fiber (OPTICS LETTERS / Vol. 30, No. 24, 2005)

The HLPG refers to a fiber where there exists a periodical screw-type index-modulation along the fiber axis. Compared with the conventional LPG fabricated by using the point-to-point writing technique, the HLPG have some advantages, such as low polarization dependence loss (PDL); the low cost in terms of the fabrication setup; and the inherent helical-characteristics which are especially suitable for controlling the dispersion, loss, angular momentum, and polarization state of light in optical fiber. Recently, HLPG has attracted a great research interest and has found many potential applications, such as the lateral stress, temperature, and torque sensors, all-fiber band-rejection filter, mode-converter for micromanipulation, and conversion of orbital angular momentum beams [1-9].

In the following, firstly, we will develop a new kind of method to fabricate the helical-type LPG. Secondly, we will make qualitative analysis on the forming mechanism of the HLPG. Finally, based on the hypothesis of the core-eccentricity mechanism, we will discuss the phase-matching conditions through the coupled-modes theory for this kind HLPGs.

5.2 Fabrication setup and results of the HLPG

Figure 5.2.1 shows fabrication setup of the HLPGs, which consists of a CO_2 laser, three translation stages, a fiber rotation motor, and a testing system for measuring the transmission spectrum the fabricated HLPG, where the utilized CO_2 laser (SYNRAD-100) works at a high repetition rate of 5 kHz with the maximum output power of 100 W and its duty-cycle can be changed between 1 to 99%. To fabricate H-LPFG, firstly, the selected fiber (fixed at the clamp and the center of rotator) is homogenously heated to its fused status through a sapphire tube, meanwhile the heated fiber is homogenously twisted through the rotation motor (ThorLabs: PRM1/MZ8). Noted that as shown in Fig. 5.2.1, the sapphire tube is fixed at a spatial site but the fiber is not fixed, which can continuously move through the tube by driving the motored stage 3 (ThorLabs: MTS50/M). Period of the HLPFG is precisely controlled by the speeds of both the fiber-moving stage and the rotator. Moreover, the two translation stages 1 and 2 can provide a little longitudinal stress to the fiber so that to make the fiber straight all the time during the fabrication process. Here it must be pointed that unlike the previous methods where a ZnSe lens was generally utilized in order to focus the CO_2 laser beam directly onto the fiber and thus decrease the laser power (but as a negative result, the fiber transverse section cannot be homogeneously heated), here a sapphire tube (to be used as a miniature oven with a constant temperature inside) is specially designed and utilized in place of the focused lens. Since the sapphire tube rather than the fiber is directly heated by the CO_2 laser, the passed fiber within the tube region can be homogeneously heated. As a result, HLPGs can easily and repeatedly be obtained with a high yielding-rate.

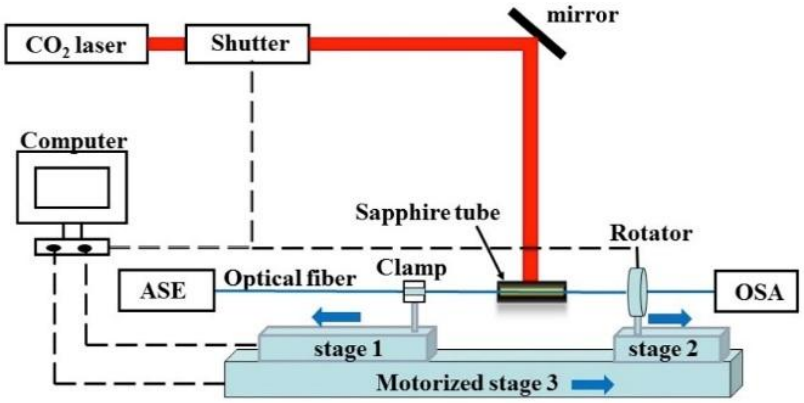

Fig. 5.2.1. Experimental setup for fabrication of the HLPG based on CO2 laser

By using the above setup, we had fabricated several kinds of the HLPGs with different periods. Figure 5.3.1 shows the transmission spectrum of a typical HLPG, where the grating period adopted is 648 μm, the grating length is 22.68 mm, and the power of the CO_2 laser what we use is nearly 35W. From this figure, one can obviously see that at 1573.5 nm, there really exist a strong loss peak and the overall loss beyond the loss-band is smaller than 1dB, which in return means that the proposed helical-type LPGs and its fabrication method all are available in practice.

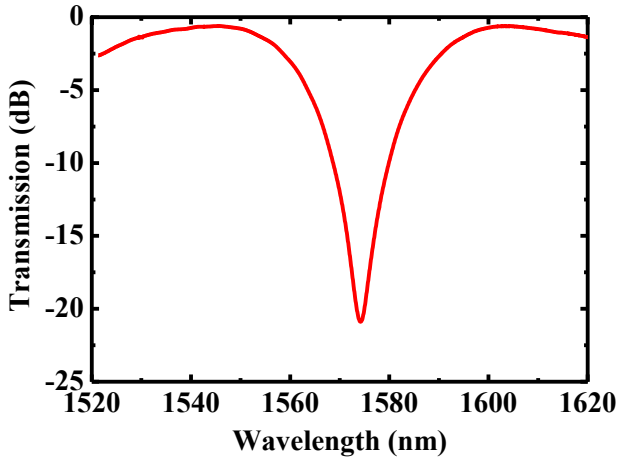

Fig. 5.2.2. Transmission spectrum of a fabricated HLPG

We further performed some torsion test for the twisted performances of the HLPG in

order to explore its potential application to the torque sensor. We measured the transmission spectra of the fabricated HLPG under 9 different torsional angles (i.e., -360°, -270°, -180°, -90°, 0°, 90°, 180°, 270°, and 360°) at room temperature, which are shown in Fig. 5.2.3. We set the rotation direction of fabricated HLPG as the positive direction. It is very interesting to find that when the fabricated HLPG is twisted in the positive direction, the attention peak shift to the short wavelength side; when the fabricated HLPG is twisted in the negative direction, the attention peak shift to the long wavelength side. And torsional responsivity is -3.59 pm/deg, which is the same level as those reported in [10].

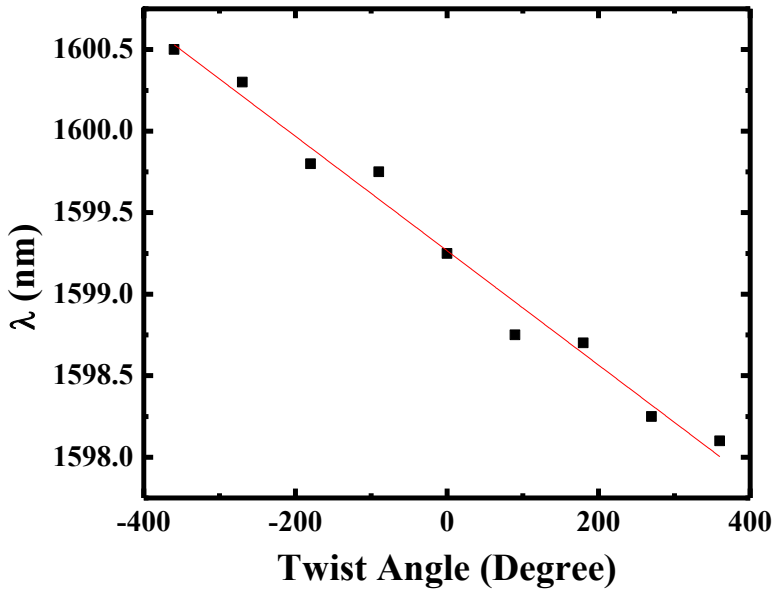

Fig. 5.2.3. Torsion characteristics of the fabricated HLPG

5.3 Principle and mechanisms for the formation of the HLPG

We used the microscope to check the surface of the fabricated HLPG. Figure 5.3.1 is microscope image of one of the fabricated HLPG. From this figure, it is found that the fabricated HLPG have a clear surface, i.e., any defects previously existed in those written by using point-to-point CO_2 laser cannot be found. To confirm the above result, we have done the same measurements but using atomic force microscope (AFM), the result is shown in Fig. 5.3.2, where the image area is about 10μm × 70μm. It is found that there really existed a clear helical structure with a constant pitch on the shallow surface of the HLPG, which makes us believe that there may have the following two mechanisms to form the periodical index-modulation in the core of HLPG.

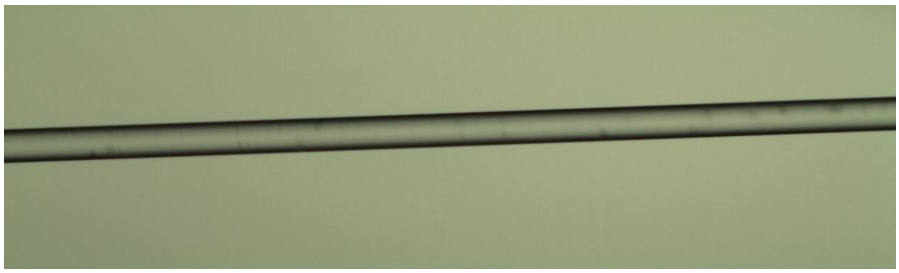

Fig. 5.3.1. The image of fabricated HLPG by using microscope

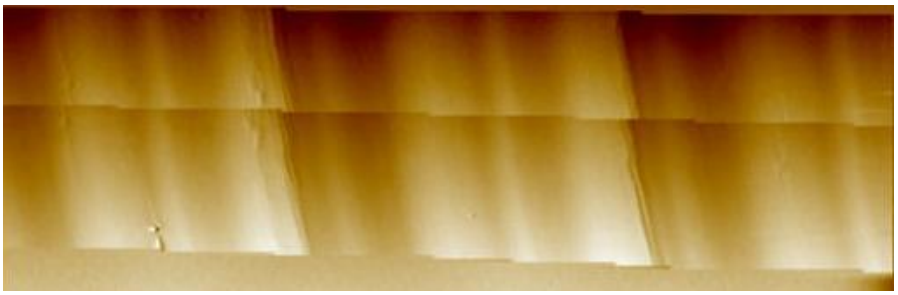

Fig. 5.3.2. The image of HLPG by using AFM

I. Residual stress relaxation

Although there are no significant deformations on the surface of fabricated HLPG, we believe that the refractive index-change of the HLPG may be related to the effect of the residual stress relaxation in the fiber. During the fabrication processes, we make use of

a weight to provide a longitudinal stress to fiber and make use of a rotation stage to provide transverse stress to fiber. When the forward side of the rotated fiber in the molten status, the transversal stress and longitudinal stress become the stress in the helical direction. It is well known that the stress applied axially to a fiber will result in a refractive-index change to the fiber core, which is expressed by

$$\Delta n = \frac{n^3}{2E}(1+\nu)(\rho_T + \rho_L)\Delta\sigma, \tag{5.3.1}$$

where n is the refractive index of the core; E is the Young`s modulus, ν is the Poisson`s ratio, $\Delta\sigma$ is the sum of stress, the ρ_T and ρ_L are the photoelastic tensors, respectively. According the same principle, one can naturally think that a helical type index-change could be produced due the existence of the helical-type stress produced in HLPG.

II. Core's eccentricity

For the conventional single-mode fiber, due to the tolerances of the fiber`s fabrication setup, it is impossible to keep the core diameter of the fiber always the same, there generally exists some random deviations to the fiber core with the range of ±1 μm or even more. Moreover through the fabrication process of HLPG, we periodically twist the fiber under the molten status, which will inevitably enhance the eccentricity of the fiber core and thus results in periodic refractive index changes. This is very similar like the single helical chiral fiber [11] as shown in Fig. 5.3.3.

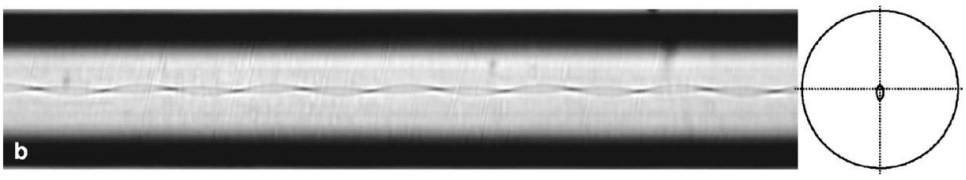

Fig. 5.3.3. Side image and schematic of face image of the single-helix grating studied (J. Opt. Soc. A. B/Vol. 24, No. 10, 2007)

In the above, two probable explanations for the formation mechanism of the HLPG are addressed. Beyond these, there may exist other unknow mechanisms which absolutely need further study in the near future.

5.4 The coupled-modes theory for the helical-type LPG

In this section, we will further investigate the modes-coupling and the phase-matching conditions in a HLPG in theory. According to the assumption of the core`s eccentricity in the HLPG, the core boundary profile $r_{co}(\theta, z)$ for the HLPG can be expanded in harmonic functions [12]:

$$r_{co}(\theta, z) = r_0 + \sum_n r_n \cos(n\theta - nk_u z) \tag{5.4.1}$$

Because of the fabricated HLPG is single helical structure, the Eq. (3.2.3) can be simplified as Eq. (5.4.2) [11]

$$\frac{dA_j}{dz} = i\sum_k A_k(z)\{\exp[i(\beta_k - \beta_j - k_u)z]W_{j,k}^{+} + \exp[i(\beta_k - \beta_j + k_u)z]W_{j,k}^{-}\}, \tag{5.4.2}$$

where the k_u is the helical pitch, and the $W_{j,k}^{+}$ and $W_{j,k}^{-}$ are the matrix elements of perturbation operator, which are given by

$$W_{j,k}^{+} = \frac{1}{2}\Delta\varepsilon r_0 r_1 \int_0^{2\pi} d\theta \vec{E}_j^{*} \cdot \vec{E}_k(\theta, r_0) e^{i\theta} \tag{5.4.3}$$

$$W_{j,k}^{-} = \frac{1}{2}\Delta\varepsilon r_0 r_1 \int_0^{2\pi} d\theta \vec{E}_j^{*} \cdot \vec{E}_k(\theta, r_0) e^{-i\theta} \tag{5.4.4}$$

From Eq. (5.4.3) and Eq. (5.4.4), it is easily seen that $W_{j,k}^{+} = W_{j,k}^{-*}$ is satisfied.

It is important to note that the perturbation operator $\widehat{W}_\delta$ is singular: it is proportional to $\delta(r - r_0)$. Therefore, its matrix elements $W_{j,k}^{+}$ and $W_{j,k}^{-}$ are evaluated on the surface of

the core-cladding interface. One well-known implication of this singularity [13] is that the integrals in Eqs. (5.43) and (5.44) are ill defined because the radial components of the electric filed $\vec{E}_k$ and $\vec{E}_j$ are discontinuous. In other words, there is an ambiguity in which value of the radial electric field E_r should be used: the one inside or outside the core. Well-established prescriptions [13] for choosing the proper value of E_r exist, and other alternative techniques employing curvilinear coordinates have been developed recently [14]. The radio between the two values is $E_r^{in}/E_r^{out} = \epsilon_{cl}/\epsilon_{co}$. Therefore, when the index contrast between the core and cladding is small, as assumed below, the ambiguity in evaluating the integrals in Eqs. (5.43) and (5.44) disappears.

Next, we briefly review their classification and derive their propagation properties in the limit of a wide-cladding radius $R_{cl} \gg \lambda$ for the cladding modes and small index contrast $|n_{co} - n_{cl}| \ll n_{cl}$ for the core modes.

Firstly, we consider the core modes. The size of the core and the dielectric permittivity contrast between the core and cladding determine the number of modes confined by the core. Quantitatively, this number is determined by the so-called fiber parameter $V_{co} = k_0 r_0 \sqrt{\epsilon_{core} - \epsilon_{cl}}$. For $V_{co} < 2.406$, the fiber is single mode, supporting a single doubly degenerate propagating electromagnetic mode. Double degeneracy arises because the mode can be either x- or y-polarized. These two polarizations can be combined to produce two degenerate circularly polarized modes: right-hand circularly polarized (RCL) and left-hand circularly polarized (LCP) modes. The naming convention for these modes is HE_{11} or LP_{01}.

The physical meaning of this notation is as follow. The HE classification refers to the symmetry and nodal properties of the axial fields H_z and E_z. The name HE_{11} implies that the modes possess non-vanishing H_z and E_z, and that the azimuthal dependence of fields is $e^{\pm i\theta}$ for RCP and LCP modes, respectively. The dispersion relation of the HE_{11} core mode is implicitly given by

$$\frac{J_0(u_{co})}{u_{co}J_1(u_{co})} = \frac{K_0(w_{co})}{w_{co}K_1(w_{co})}, \tag{5.4.5}$$

Where $u_{co} = r_0\sqrt{k_0^2 n_{co}^2 - \beta_{co}^2}$ and $w_{co} = r_0\sqrt{\beta_{co}^2 - k_0^2 n_{cl}^2}$. Numerically solving for u_{co} and w_{co} yields the propagation constant of the core doublet β_{co}. Eq.(5.4.5) is derived under the approximation of infinitely extended cladding.

In the small contrast limit, the electric field components of the circularly polarized LP_{01} core eigenmode are given by the following expressions: inside the core, for $0 \le r \le r_0$:

$$\begin{aligned} E_r &= -i\frac{\beta_{co} r_0}{\sqrt{2}u_{co}} J_0\left(\frac{u_{co}}{r_0}\right) e^{\pm i\theta} \\ E_\theta &= \pm\frac{\beta_{co} r_0}{\sqrt{2}u_{co}} J_0\left(\frac{u_{co}}{r_0}\right) e^{\pm i\theta} \\ E_Z &= \frac{1}{\sqrt{2}} J_1\left(\frac{u_{co}}{r_0}\right) e^{\pm i\theta}, \end{aligned} \tag{5.4.6}$$

and inside the cladding, for $r > r_0$:

$$\begin{aligned} E_r &= -i\frac{\beta_{co} r_0}{\sqrt{2}u_{co}} \frac{J_0(u_{co})}{K_0(w_{co})} K_0\left(\frac{w_{co}}{r_0}\right) e^{\pm i\theta} \\ E_\theta &= \pm\frac{\beta_{co} r_0}{\sqrt{2}u_{co}} \frac{J_0(u_{co})}{K_0(w_{co})} K_0\left(\frac{w_{co}}{r_0}\right) e^{\pm i\theta} \\ E_Z &= \frac{J_1(u_{co})}{\sqrt{2}K_1(w_{co})} K_1\left(\frac{w_{co}}{r_0}\right) e^{\pm i\theta}, \end{aligned} \tag{5.4.7}$$

where u_{co} and w_{co}, and β_{co} of the core modes are obtained by numerically solving Eq. (5.4.5); the + (-) sign of the harmonic angular dependence corresponds to LCP (RCP) waves, respectively.

Secondly, the influence of a very small core $r_0 \ll R_{cl}$ on the fields` structure of the cladding modes is negligible for the lowest-order cladding modes. Defining the cladding fiber parameter as $V_{cl} = k_0 R_{cl}\sqrt{\epsilon_{cl} - 1}$, considerable simplifications can be obtained in limit of $V_{cl} \gg 1$. The exact expressions for the electric and magnetic fields of an arbitrary cladding mode, as well as their exact dispersion relations, can be found in [13, 15]. Here, in the relevant limit of $V_{cl} \gg 1$, we only concentrate on several modes that are coupled to the HE_{11} core modes through the selection rules that follow from Eqs. (5.4.3) and (5.4.4). The relevant cladding modes belong to two distinct types: (a) the doubly degenerate band LP_{0n} consisting of HE_{1n} cladding modes (where $n \gg 2$), and (b) an almost-degenerate quartet band LP_{1n} consisting of TE_n and TM_n, and doubly degenerate HE_{2n} modes. Because of the fabricated HLPG is single helical structure, the LP_{1n} cladding quartet is coupled to the LP_{01} core band.

The LP_{1n} quartets consist of the TE_n and TM_n, and the doubly degenerate HE_{2n} modes. In the limit of the small low-contrast fiber core $V_0 \ll V_{cl}$ and wide fiber $V_{cl} \gg 1$ the dispersion relations of all four modes of the nth quartet can be computed from $J_1(u) = 0$, where $u = R_{cl}\sqrt{k_0^2 n_{cl}^2 - \beta^2}$. The propagation constant β of the nth quartet modes is given by

$$\beta_{LP_{1n}} = \sqrt{k_0^2 n_{cl}^2 - \frac{j_{1n}^2}{R_{cl}^2}} \approx k_0 n_{cl} - \frac{j_{1n}^2}{2k_0 n_{cl} R_{cl}^2}, \tag{5.4.8}$$

where j_{1n} is the nth root satisfying $J_1(j_{1n}) = 0$.

For completeness, we present the electric field components of the TE_n, TM_n, and HE_{2n} modes. These formulae are valid in the small-core and large-core approximation. For the TE_n modes, the only non-vanishing component of the electric field is $E_\theta = J_1(j_{1n} r/R_{cl})$. For the TM_n modes, the non-vanishing components of the electric field are $E_z = J_0(ur/R_{cl})$ and $E_r = i\beta_{LP_{1n}} R_{cl} J_1(j_{1n} r/R_{cl})/j_{1n}$. Finally, for the HE_{2n} modes we

find that $E_r = -i\beta_{LP_{1n}} R_{cl} J_1(j_{1n} r/R_{cl}) e^{\pm 2i\theta}$, $E_\theta = \pm\beta_{LP_{1n}} R_{cl} J_1(j_{1n} r/R_{cl}) e^{\pm 2i\theta}$, and $E_z = j_{1n} J_2(j_{1n} r/R_{cl}) e^{\pm 2i\theta}$, where $\pm$ corresponds to the LCP (RCP) modes, respectively.

The strength of the coupling between modes j and k depend on the value of the $W_{j,k}^{\pm}$. This value of $W_{j,k}^{+}$ is non-vanishing only when the following selection rule is satisfied: $-M_j + M_k + 1 = 0$, where M_j and M_k are the modes` azimuthal numbers: the E_z and H_z components of the modes have $\exp(iM\theta)$ dependence. This relation constitutes the selection rule for the RCP. Likewise, the selection rule for the LCP is $-M_j + M_k - 1 = 0$.

The effectiveness of mode coupling depends not only on the magnitude of the transition matrix operator, but also on the satisfaction of the chiral equivalent of the Bragg scattering conditions. From Eq. (5.4.2), these are $\beta_k - \beta_j = k_u$ for the RCP and $\beta_k - \beta_j = -k_u$ for the LCP.

The RCP-polarized j_{th} mode coupling to the TE_n and TM_n modes via the $W_{j,k}^{-}$ matrix element. These two cladding modes can belong to any of the LP_{1n} cladding mode quartets. Examples of these modes belonging to the LP_{11} band are shown in the top panel of figure 5.4.1. the coupling is resonant if the helical pitch is chosen to be $k_u = \beta_{co} - \beta_{LP_{1n}}$. The LCP core mode is coupled to the HE_{2n} cladding mode. Note that the HE_{2n} cladding mode belongs to the same almost degenerate quartet LP_{1n} as TE_n and TM_n. As shown below, the coupling strength of the LCP core mode to the HE_{2n} is the same as the coupling strength of the RCP core mode to the TE_n / TM_n modes.

The coupling amplitudes of the RCP core mode to the TE_n and TM_n modes can be calculated by assuming the approximate unperturbed profiles of the core and cladding modes calculated in the small-core large-cladding approximations. We find that these two coupling strength, W_{TM}^{-} and $W_{TE}^{-} \equiv W_{co^{RCP}TM_n}^{-}$, are related to each other through $W_{TM}^{-} = iW_{TE}^{-}$, and can calculated as

$$W_{co^{RCP}TM_n}^{-} = \frac{(\epsilon_{co} - \epsilon_{cl})r_1}{2\sqrt{2}R_{cl}} \sqrt{\frac{\beta_{co}\epsilon_{cl}}{\beta_{LP_{1n}}}} \frac{J_0(u_{co})J_1(j_{1n}r_0/R_{cl})}{u_{co}j_{1n}} \times A_{co}A_{LP_{1n}}, \tag{5.4.9}$$

where the normalization constant A_{co} and $A_{LP_{1n}}$ for the LP_{1n} mode is given by

$$|A_{co}|^2 = \frac{\epsilon_{co}}{u_{co}^2}[J_0^2(u_{co}) + J_1^2(u_{co})] + \frac{\epsilon_{cl}}{w_{co}^2}\frac{J_1(u_{co})}{K_1(w_{co})}[K_1^2(w_{co}) + K_0^2(w_{co})] \tag{5.4.10}$$

$$\left|A_{LP_{1n}}\right|^2 = \frac{\epsilon_{cl}}{j_{1n}^2}J_0(j_{1n})J_2(j_{1n}). \tag{5.4.11}$$

Note that $\left|A_{LP_{1n}}\right|^2$ is always positive because of the interlacing of the Bessel function roots [16]: zeros of the J_1 Bessel function always fall between the zeros of the J_0 and J_2 Bessel functions.

It is straightforward to show that an RCP core mode with amplitude a_{co} simultaneously coupled to two resonant modes with the coupling strengths W_{TM}^{-} and W_{TE}^{-} evolves according to the equation $d^2a_{co}^{RCP}/d\tilde{z}^2 + (|W_{TM}^{-}|^2 + |W_{TE}^{-}|^2)a_{co}^{RCP} = 0$, so the effective interaction constant for the RCP core mode is $WW_{co^{RCP}}^{-} = \sqrt{2}W_{co^{RCP}TM_n}^{-}$.

Now we consider the interaction of the LCP core mode with the LP_{1n} band. As explained earlier, the LCP core mode is coupled to the HE_{2n} cladding mode of the LP_{1n} quartet. The coupling coefficient $W_{HE_{2n}}^{-}$ is calculated to be

$$W_{co^{RCP}HE_{2n}}^{-} = \frac{(\epsilon_{co} - \epsilon_{cl})r_1}{2R_{cl}} \sqrt{\frac{\beta_{co}\beta_{LP_{1n}}}{{k_0}^2}} \frac{J_0(u_{co})J_1(j_{1n}r_0/R_{cl})}{u_{co}j_{1n}} \times A_{co}A_{LP_{1n}}, \tag{5.4.12}$$

which can be shown to be exactly equal to the $\sqrt{2}W_{co^{RCP}TM_n}^{-}$ in the large-cladding limit of

$\beta_{LP_{1n}} = n_{cl}k_0$ that follows from Eq. (5.4.8). Thus, we predict that the LCP core mode oscillates with the same spatial period as the RCP core mode. Therefore, it is predicted that a large-radius single-helix LPG is polarization insensitive, i.e. the circular dichroism/birefringence is very small.

5.5 Summary

In this chapter, firstly a simple review on the developments of the HLPG to date has been introduced. Secondly, a new kind of method to fabricate this kinds of gratings has been proposed and successfully demonstrated, which is based on the utilization of a CO_2 laser combined with a sapphire tube technique. Thirdly, a qualitative analyses on the forming mechanism of the proposed HLPG have been addressed. Finally, we make a qualitative analysis of the mechanism of forming HLPG. Finally, based on the hypothesis of the core-eccentricity mechanism, coupled-modes equations for the HLPG have also been discussed.

References

[1]. C. D. Pool, C. D. Townsend, and K. T. Nelson, "Helical-grating two-mode fiber spatial-mode coupler," J. Lightwave Technol. 9, 598–604 (1991).

[2]. V. I. Kopp, V. M. Churikov, J. Singer, N. Chao, D. Neugroschl, and A. Z. GenacK, "Chiral fiber gratings," Science 305, 74-75 (2004).

[3]. S. Oh, K. Lee, U. Paek, and Y. Chung, "Fabricatin of helical long-period fiber gratings by use of a CO_2 laser," Opt. Lett. 29, 1464-1466 (2004).

[4]. W. Shin, B. Yu, Y. Noh, Z. Lee, and D. Ko, "Bandwidth-tunable band-rejection filter based on helicoidal fiber grating pair grating of opposite helicitied," Opt. Lett. 32, 1214-1216 (2007).

[5]. Ivanov, "Fabrication of long-period fiber gratings by twisting a standard single-mode fiber," Opt. Lett. 30, 3290-3292 (2005).

[6]. L. Xian, P. Wang, and H. Li, "Power-interrogated and simultaneous measurement of

temperature and torsion using paired helical long-period fiber gratings with opposite helicities," Opt. Express 22, 20260-20267 (2014).

[7]. C. N. Alexeyev, T. A. Fadeyeva, B. P. Lapin, and M. A. Yavorsky, "Generation and conversion of optical vortices in long-period twisted elliptical fibers," Appl. Opt. 51, C193-C197 (2012).

[8]. H. Xu and L. Yang, "Conversion of orbital angular momentum of light in chiral fiber gratings," *Opt. Lett.* 38, 1978-1980 (2013).

[9]. Y. Rao, Y. Wang, Z. Ran, and T. Zhu, "Novel fiber-optic sensors based on long-period fiber gratings written by high-frequency CO_2 laser pulses," J. Lightwave Technol. 21, 1320-1327 (2003).

[10]. B. Song, Y. Miao, W. Lin, H. Zhang, J. Wu, and B. Liu, "Multi-mode interferometer-based twist sensor with low temperature sensitivity employing square coreless fibers," Opt. Express 21(22), 26806–26811 (2013).

[11]. V. I. Kopp, V. M. Churikov, G. Zhang, et al, "Single- and double-helix chiral fiber sensors," J. Opt. Soc. Am. B. 24, A48-52 (2007).

[12]. G. Shvets, S. Trendafilov, V. I. Kopp, et al, "Polarization properties of chiral fiber gratings," J. Opt. A: Pure Appl. Opt 11, 1-10 (2009).

[13]. Snyder A and Love J, "Optical Waveguide Theory (London: Chapman and Hall)," (1983).

[14]. Skorobogatiy M, Johnson S, Jacobs S and Fink Y, "Dielectric profile variations in high-index-contrast waveguides, coupled mode theory, and perturbation expansions," Phys. Rev. E 67, 046613 (2003).

[15]. Okamoto K, "fubdamentals of optical waveguides (San Diego, CA: Academic)," (2000).

[16]. Abramowitz M and Stegun I A, "Handbook of mathematical functions with formulas, graphs, and Mathematical Tables (New York: Dover)," (1965).

6 Helical LPG formed in thinned fiber and its application to refractometric sensor

6.1 Introduction

In the past few decades, long-period fiber grating (LPG)-based fiber sensors including the refractometric sensors have been comprehensively studied and widely used in the fields of civil engineering, industry, biomedicine, and chemistry, etc. [10-15]. However, the refractive index measure- ments based on the utilization of HLPG (with extremely low polarization-dependence loss) have rarely been reported. Furthermore, it is commonly known that for LPG-based sensing systems, since the resonant wavelength is very sensitive to both the external temperature and the ambient refractive index, there always exist such need to develop a simple technique enabling to discriminate both of these effects simultaneously. Temperature-insensitive measurement for the ambient refractive-index is strongly desired to practical application and thus being an important research topic.

In this chapter, a new kind of HLPG written by using CO_2 laser technique is proposed and experimentally demonstrated, where a sapphire tube is particularly utilized in place of the focal lens. Although the sapphire tube technique has already been reported and successfully demonstrated for the fabrication of micro /nano fiber [16], this is the first report to fabricate the thinned HLPGs with this technique. The proposed method allows to fabricate HLPGs with a diameter less than several tens of micrometer. In order to compare with the experimental results, theoretical simulations have also been done, which are related to changes of the resonant wavelengths of HLPGs under the condition of three different fiber diameters. Furthermore, as an application of this kind of HLPGs, a novel HLPGs-based refractometric sensor that allows for temperature-free measurement of the refractive index is proposed and experimentally demonstrated.

6.2 Experiment setup of the Helical LPG

The same setup as shown in Fig. 5.2.1 was adopted here. However, in the experiments conducted in this study, three kinds of thinned fibers with diameter of 114, 103, and 92 μm, respectively, were utilized to fabricate the HPLGs. These three kind of thin fibers had been made in advance by tapering the conventional SMF fibers (FutureGuide®-SR15E, Fujikura Inc.), which have a cladding and core diameters of 125 and 8.2 μm, respectively. For more details, while the conventional SMF was homogenously heated through the sapphire tube, it was tapered and drawn simultaneously by driving the motored stages 1 and 2 but the rotator and stage 3 were kept inactive. With using this method, diameter of the resulted fiber can easily be controlled by only adjusting the stretching length of the fiber. Moreover, based on the above fabrication processes, it is rational for us to assume that the core diameter of the thinned fiber should proportionally changes in accordance with decrement of the cladding diameter. Therefore for the thinned fibers (with a diameter of 110, 103 and 92 μm, respectively) utilized in our case, the corresponding core diameters should be 7.22, 6.76, and 6.10 μm, respectively.

Once if the thinned fiber was successfully obtained, this fiber was then continuously rotated at a speed of 25^{o}/s by driving the rotator and meanwhile the fiber moved through the sapphire tube at a constant speed of 46 μm/s, which was controlled by the translation stage 3. After the time of 750 s until all the stages stopped, the HLPG was then obtained with a grating period of 828 μm and length of 34.5 mm, respectively. All the above procedures were pre-programmed and controlled through a computer with the LabView software.

To make sure the fabrication of these three kinds of HLPGs successful, we then measured their transmission spectra by using the setup shown in Fig. 6.2.1, where an amplified spontaneous emission (ASE) source and an optical spectral analyzer (OSA) were utilized. Figure 6.2 shows the measuring results of the three HLPGs (with a diameter of 110, 103, and 92 μm, respectively). It can be seen that that there really exist three individual notches (loss band), each of which has a depth of 20.58, 17.76 and 14.99 dB, respectively,

and the corresponding peak wavelengths are 1608.80, 1574.50, and 1539.60 nm, respectively. Since these notches show no differences with those obtained from the conventional LPGs, they are certainly attributed to the coupling between the fundamental mode and the forward high-order cladding modes. Unlike the previous HLPGs reported in Ref. [4], the surface deformation cannot be found in our gratings, which in return means that the formation mechanism of the fabricated HLPGs may be attributed to the residual-stress releasing in the pristine fiber rather than the surface deformation [5]. Moreover, it can be seen that diameter of the HLPG will strongly affect the spectral properties of the fabricated HLPG itself and obviously, the notch will shift largely to the short wavelength once if the fiber diameter is decreased. These results certainly make us to believe that one can find some new applications of the thinned HPLG in fiber sensing field.

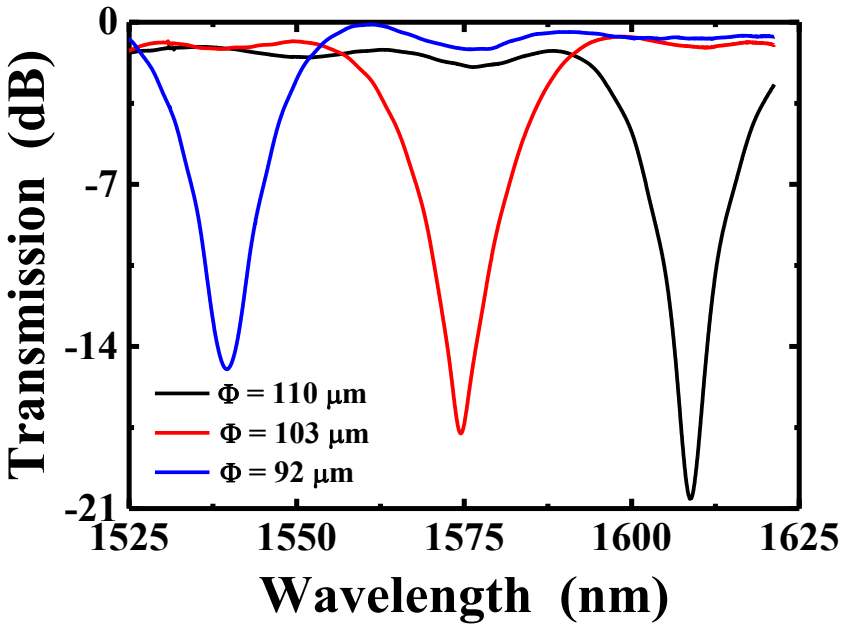

Fig. 6.2.1. Transmission spectra of the three different HLPGs measured at room temperature

6.3 Numerical analyses for the resonant coupling between the core and cladding modes in Helical LPG

To verify the above experimental results, we had done some of simulations by numerically investigating the resonant wavelengths for the coupling between the core and cladding modes. For convenience, we assume that the fiber used is a simple three-layer with step-index. In general, solution to the resonance wavelengths of the cladding modes are somewhat complicate and one can obtain them by solving the dispersion equation given in [17] under the condition of phase matching. In what follows, we limit the calculation to a HPLG where nonzero coupling for core-cladding mode occurs only between the core mode (HE_{11}) and the hybrid cladding modes with azimuthal number l=1. More specifically, all the parameters of the three utilized thin fibers, such as the radii of the core a_1 and cladding a_2, the refractive indexes of the core n_1 and cladding n_2, and the surrounding material n_3, are particularly chosen as: a_1=3.61, 3.38, and 3.05 μm, respectively, a_2=110, 102, and 92 μm, respectively, and n_1=1.4580, n_2=1.4536, n_3=1.0 (the surrounding material is assumed to be air with index equal to 1). Period of the grating is assumed to be 828 μm. For comparison, two other grating periods of 778 and 878 μm are utilized in the calculations. By solving the dispersion equation of (5) in [17], we have obtained a sets of resonant wavelengths related to the cladding modes with azimuthal number l=1, i. e. HE_{1v}, but only the HE_{13} mode is within the wavelength range of 1525-1650 nm when the grating period of 828 μm (which was the same as we used in experiment) is selected, which in return means the spectral notches appeared in Fig. 6.2.1 could be attributed to the coupling between the core mode and the HE_{13} cladding mode. Figure 6.3.1 shows the calculated results for relationship between the resonant wavelength and the diameter of the thinned fiber. The blue, red, and black curves correspond to the results where the grating periods are 778, 828, and 878 μm, respectively. Note that only the notch resulted from the HE_{13} cladding mode is considered here within the wavelength range of our interest. It is seen that the resonant wavelength will shift largely to short wavelength direction once if the cladding diameter is decreased, this tendency is exactly the same as the experimental results shown in Fig. 6.2.1. From Fig.

6.3.1, it can also be found that for the cladding diameters of 110, 103, 92 μm, and the grating period of 828 μm, the corresponding resonant wavelengths are 1613.0, 1580.0, and 1539.0 nm, respectively, these results agree very well with those experimental ones (i.e., 1608.80, 1574.50, and 1539.60 nm shown in Fig. 6.2.1), which in return means that the calculation model and all the assumed parameters in this study are pretty reasonably.

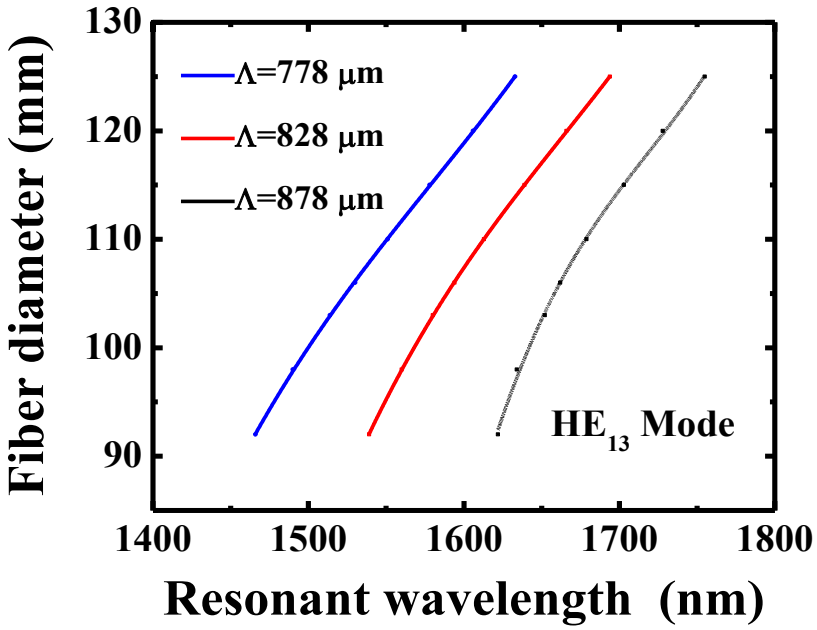

Fig. 6.3.1. Calculated results for dependence of the peak wavelength of the HE_{13} loss notch on fiber diameter under three different grating periods

6.4 Principle and measurement results of the helical LPGs-based refractometric sensor

By using the same setup as shown in Fig. 5.2.1, we furtherly wrote two cascaded HLPGs on a same SMF where one grating was taped with a diameter of 110 μm and the other was taped with a diameter of 92 μm. To find the possibility of this kind of fiber grating utilized as a refractometric sensor, we had investigated the responsivities of HLPGs for both the temperature and the ambient refractive index in our experiment.

To investigate the thermal performance, these two cascaded HLPGs were firstly placed in a temperature chamber, where the temperature can be discretely changed from 20 to 150 ^{o}C with a resolution of ±1 ^{o}C. Then we measured the transmission spectra at six different temperatures (i.e., 20, 40, 60, 80, 100, and 120^{o}C, respectively). The measuring results are shown in Fig. 6.4.2. It is seen that as the temperature is increased, the spectrum is linearly shifted to long-wavelength direction with a responsivity of ~52 pm/^{o}C, which is almost the same level as that reported in [6]. However it can be found that the wavelength separation $\Delta\lambda$ labeled in Fig. 6.4.1 is temperature- insensitive one, which almost remain constant. To show this phenomenon more clearly, we plotted the Fig. 6.4.1 again as Fig. 6.4.2, which directly shows changes of the peak-wavelength separation $\Delta\lambda$ (as defined in Fig. 6.4.1) vs. the temperature changes. Form Fig. 6.4.2, it is obviously seen that $\Delta\lambda$ is totally temperature-insensitive and almost remains a constant whenever the temperature is changed between 20 to 120 ^{o}C.

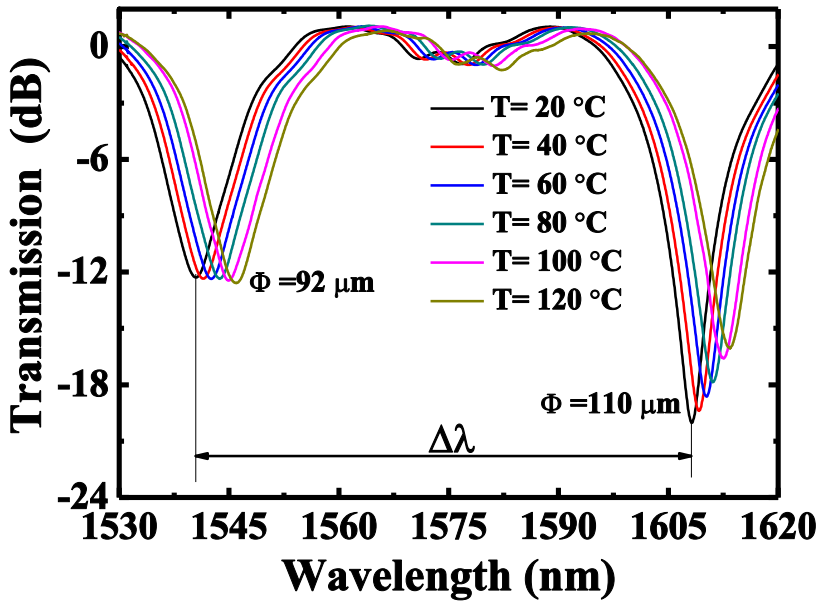

Fig. 6.4.1. Transmission spectrum of the two cascaded HLPGs under six different temperatures

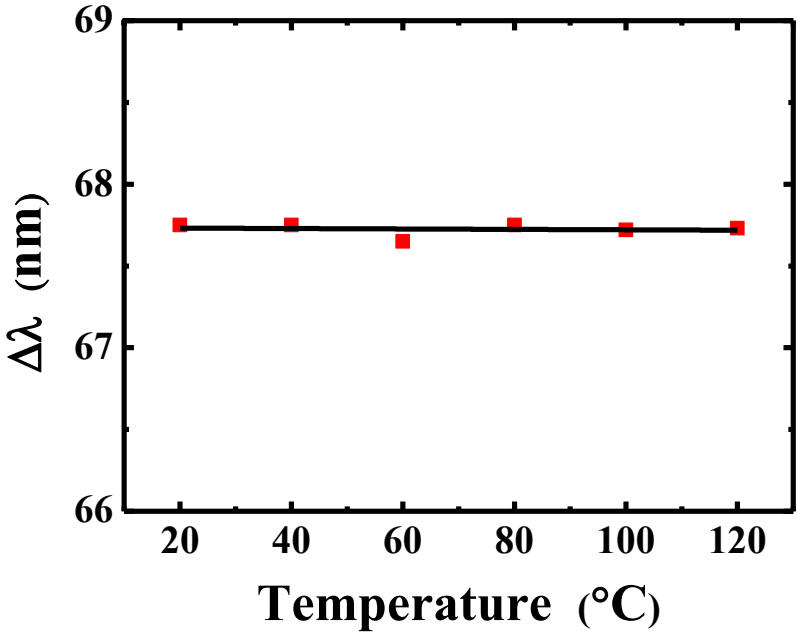

Fig. 6.4.2. Dependence of the peak-wavelength separation Δλ on temperature

Base on the above fact, it is believed that the proposed cascaded HLPGs can be

utilized to measure the refractive index of the surrounded solution but without any temperature cross-effects. The basic principle is that although the magnitude $\Delta\lambda$ shown in Fig. 6.4.1 is temperature-insensitive one, it would be highly sensitive to change of the refractive index of the surrounded material, because the two cascaded HLPGs have different diameters and thus when the refractive index of the ambient solution is increased, the corresponding two loss-peaks as shown in Fig. 6.4.1 will both shift to the short wavelength direction but with different amounts. To confirm this proposal, the commonly-used saline with different salt concentration of 0, 5%, 10%, 15%, 20%, and 25% (corresponding to the refractive index of 1.333, 1.343, 1.349, 1.359, 1.369, and 1.379) were employed as the ambient solutions, which were filled around the ambient region of the HLPGs. Meanwhile the room temperature at a constant was remained. Fig. 6.4.3 shows the measuring results for the transmission spectra of the two HLPGs. It is found that as the refractive index is increased, to be exactly the same as what we expected that the two loss peaks (i. e., for Φ=92 μm and Φ=110 μm) began to shift to the short-wavelength direction and each with the maximum responsivity of ~29.34 nm/RI and 21.74 nm/RI, respectively. Figures 6.4.4 shows change of the $\Delta\lambda$ in terms of the ambient refractive index, which are directly obtained from the experimental datum shown in Fig. 6.4.3, where the red rectangular symbols represent the experimental datum and the black solid curve represents the polynomial fitting one. It can be seen that just as what is expected that there really exists a one-by-one relationship between these two parameters, i. e., the refractive index and $\Delta\lambda$. Change of the $\Delta\lambda$ is about ~0.4 nm when the refractive index is changed from 1.333 to 1.379. Moreover, accuracy for the measured refractive index is estimated to be 2×10^{-4} by comparing the experimental datum and the fitted data shown in Figs. 6.4.4.

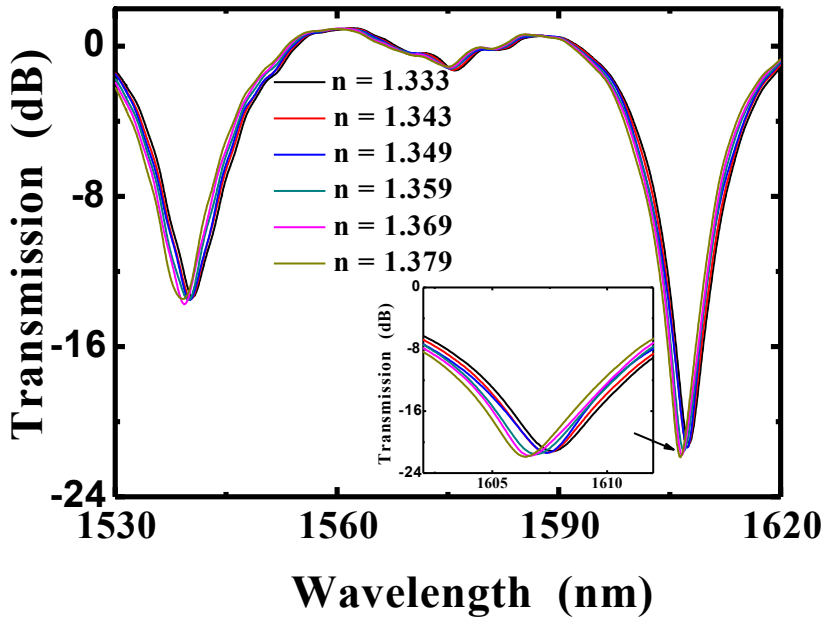

Fig. 6.4.3. Measuring results for the transmission spectra of the two cascaded HLPGs while concentration of the ambient saline solution refractive are 0%, 5%, 10%, 15%, 20% and 25%, respectively.

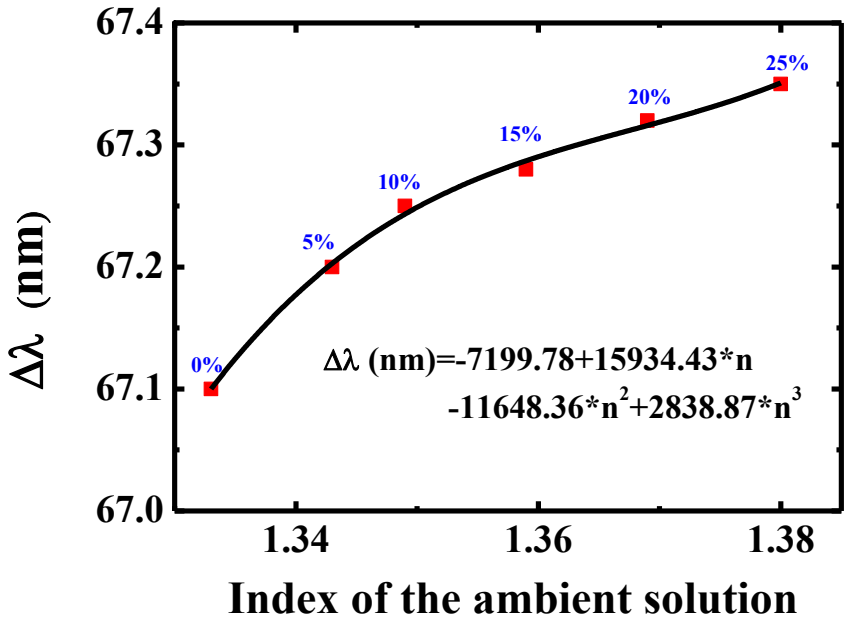

Fig. 6.4.4. Measurement results for dependent of the peak-wavelengths separation on the refractive index of the ambient solution

Finally, it must be pointed that although the wavelength responsivity obtained in this

study is rather small compared with those previous reported in Ref. [15], the proof-of-principle proposed in this study has well been accomplished. Here it is reasonable for us to expect that one can considerably increase the wavelength responsively up to 1900 nm/RI once if the diameter of the utilized HLPG can be decreased to several micrometers [15].

6.5 Summary

In conclusion, a new method enabling to fabricate HLPGs in a thinned fiber with a diameter smaller than several tens of micrometer has been proposed and experimentally demonstrated, where a sapphire tube is particularly utilized in place of the focal lens. As an application of this kind of HLPGs, a novel fiber refractometric sensor that allows for temperature-insensitive measurement of the refractive index has been proposed and successfully demonstrated. It is expected that this kind of HLPGs may find potential applications to high-sensitive fiber sensors, mode-converter and orbital angular momentum beams in optical communications.

References

[1]. C. D. Pool, C. D. Townsend, and K. T. Nelson, “Helical-grating two-mode fiber spatial-mode coupler,” J. Lightwave Technol. 9, 598–604 (1991).

[2]. V. I. Kopp, V. M. Churikov, J. Singer, N. Chao, D. Neugroschl, and A. Z. GenacK, “Chiral fiber gratings,” Science 305, 74-75 (2004).

[3]. O.V. Ivanov, “Fabrication of long-period fiber gratings by twisting a standard single-mode fiber,” Opt. Lett. 30, 3290-3292 (2005).

[4]. S. Oh, K. Lee, U. Paek, and Y. Chung, “Fabricatin of helical long-period fiber gratings by use of a CO2 laser,” Opt. Lett. 29, 1464-1466 (2004).

[5]. W. Shin, B. Yu, Y. Noh, Z. Lee, and D. Ko, “Bandwidth-tunable band-rejection filter based on helicoidal fiber grating pair grating of opposite helicitied,” Opt. Lett. 32,

1214-1216 (2007).

[6]. L. Xian, P. Wang, and H. Li, “Power-interrogated and simultaneous measurement of temperature and torsion using paired helical long-period fiber gratings with opposite helicities,” Opt. Express 22, 20260-20267 (2014).

[7]. C. N. Alexeyev, T. A. Fadeyeva, B. P. Lapin, and M. A. Yavorsky, “Generation and conversion of optical vortices in long-period twisted elliptical fibers,” Appl. Opt. 51, C193-C197 (2012).

[8]. H. Xu and L. Yang, “Conversion of orbital angular momentum of light in chiral fiber gratings,” Opt. Lett. 38, 1978-1980 (2013).

[9]. Y. Rao, Y. Wang, Z. Ran, and T. Zhu, “Novel fiber-optic sensors based on long-period fiber gratings written by high-frequency CO2 laser pulses,” J. Lightwave Technol. 21, 1320-1327 (2003).

[10]. H. J. Patrick, A. D. Kersey, and F. Bucholtz, “Analysis of the response of long period fiber gratings to external index of refraction,” J. Lightwave Technol. 16, 1606-1612 (1998).

[11]. V. Bhatia, “Applications of long-period gratings to single and multi-parameter sensing,” Opt. Express 4, 457-466 (1999).

[12]. S. W. James and R. P. Tatam, “Optical fibre long-period grating sensors: characteristics and application,” Meas. Sci. Technol. 14, R49-R61 (2003).

[13]. I. D. Villar, F. Arregui, I. Matias, A. Cusano, D. Paladino, and A. Cutolo, “Fringe generation with non-uniformly coated long-period fiber gratings,” Opt. Express 15, 9326-9340 (2007).

[14]. Y. Wang, “Review of long period fiber gratings written by CO2 laser,” J. Appl. Physics 108, 081101-081101-18 (2010).

[15]. H. Xuan, W. Jin, and M. Zhang, “CO2 laser induced long period gratings in optical microfibers,” Opt. Express 17, 21882-21890 (2009).

[16]. M. Sumetsky, Y. Dulashko, and A. Hale, “Fabrication and study of bent and coiled free silica nanowires: Self-coupling microloop optical interferometer,” Opt. Express.

12, 3521-3531 (2004).

[17]. T. Erdogan, “Cladding-mode resonances in short- and long-period fiber gratings filters,” J. Opt. Soc. Am. A 14, 1760-1773 (1997).

7. Flat-top band-rejection filter based on two successively cascaded helical LPGs

7.1 The flat-top band rejection filter and variety fabrication method

Attributed to its helicity characteristics which are especially suitable for controlling the polarization and orbit-angular-momentum state of the light in optical fiber, helical long-period fiber grating (HLPG) has attracted a great research interest and has found versatile applications, such as the temperature and torque sensors, all-fiber band-rejection filter, mode-converter for micromanipulation, and conversion of orbital angular momentum beams, etc. [1-10]. To date, various methods to fabricate the HLPG have been proposed and demonstrated, which includes the ones by homogeneously twisting a fiber with a noncircular core cross-section [1, 2] where the special fibers with a high birefringence in the core are generally demanded, and the others by creating a helical surface deformation along the fiber [3, 4] where the conventional single-mode fiber (SMF) and the point-to-point direct writing technique using on a focused CO_2 laser [11, 12] are generally used, however the fabricated HLPGs inevitably undergo the drawbacks of low yielding-rate and the weak resistance to stretching and bending, and therefore are not available to some practical applications especially for bending and strain sensors. Most recently, based on the utilization of CO_2 laser, we have proposed and developed another approach to fabricate HLPG [7, 8], where a sapphire tube is particularly utilized in place of the focal lens [13], which thus enables to robustly and repeatedly fabricate HLPGs with a high quality and moreover, even the conventional SMF fiber is available.

On the other hand, as is well known that long-period fiber grating (LPG) is one kind of fiber grating in which the strong couplings occurs only between the forward fundamental core-mode and the matched discrete cladding-modes. As a result, LPG can generally be used as an optical band-rejection filter with a bandwidth of several tens of nanometers, which is almost one to two order broader than that of fiber Bragg grating [14]. However, it is extremely difficult to precisely control the profile of the resulted notch during the LPG's

fabrication. Especially for a LPG with a broad flat-top rejection-band, although it is one of the key components and strongly desirable in fiber communication system as well as fiber sensing system, there has rarely been practically realized due to some unrealistic demands in the grating's fabrication. To date, mainly three methods have been proposed and demonstrated to realize the LPG-based flat-top filter [4, 15-21]. The first is the one based on UV exposure technique [15, 16] where the LPG is designed by using the inverse scattering method [15], as a result, the required grating' length is generally longer than 0.5 meter, which is too long to be realized due to the packaging and fabrication limitations. Furthermore, in order to obtain a flat-top type filter, sinc-like apodization is generally demanded, which is extremely difficult or even impossible to be realized by using the CO_2 laser writing technique [15, 16]. The second method is the one based on the phase-shifted LPG, where several discrete phases are assumed to insert into the LPG, as results of the simulations, flat-top rejection-band can be obtained [17-21], however how to precisely control the phase magnitude at particularly position of LPG become a critical challenge, which make this kind of LPGs not be obtained in practice until now. The third is the one based on utilization of two cascaded HLPG proposed by Shin et al. [4], in which a tunable band-rejection filter with bandwidth of several tens nanometer has been successfully obtained, however, a large separation (>10cm) between the two LPGs are adopted, the spectral interference are inevitable due to the polarization scrambling effect, as a result fluctuation of the loss-depth is so larger (>10 dB) that a flat-top band-rejection filter cannot be realized.

In this chapter, we propose and demonstrate a novel method for the fabrication of flat-top band-rejection, which is realized by fabricating two HLPGs but with opposite helicities with using CO_2 laser and the sapphire tube technique [7, 8] and successively cascading these two LPGs. The proposed HLPGs have a relative short length (less than 4.6 cm) and do not require a complex apodization in grating's amplitude, which makes this kind of HLPGs particularly suitable to be fabricated by using the robust CO_2 laser writing technique.

7.2 Measuring results for the spectrum of the cascaded helical LPGs

The same setup as shown in Fig. 5.2.1 was adopted here. In order to realize a flat-top band-rejection filter, two HLPGs which are successively cascaded but with opposite helicities were utilized here. The detailed procedures are described below. At beginning, the first section of the SMF was heated and continuously twisted to the clockwise direction (observe in the direction from right to the left side) until the cHLPG was completely fabricated, which has a grating period of 648 μm and a length of 22.68 mm (35 periods). Transmission spectrum of this grating is shown in Fig. 7.2.1(a) as labeled by black solid line. It is seen that like the general LPGs, there exists a deep notch (loss band) in the transmission spectrum, and the loss depth and its peak-wavelength are ~26 dB and 1574.50 nm, respectively, which may be attributed to the coupling between the core mode and the LP_{12} cladding mode in our case [8]. Sooner after the cHLPG was produced, the neighboring part of the utilized SMF was then successively twisted to the counterclockwise direction until the fabrication of ccHLPG was completed, which has the 640μm period and 22.4 mm grating length (i.e., cHLPG).

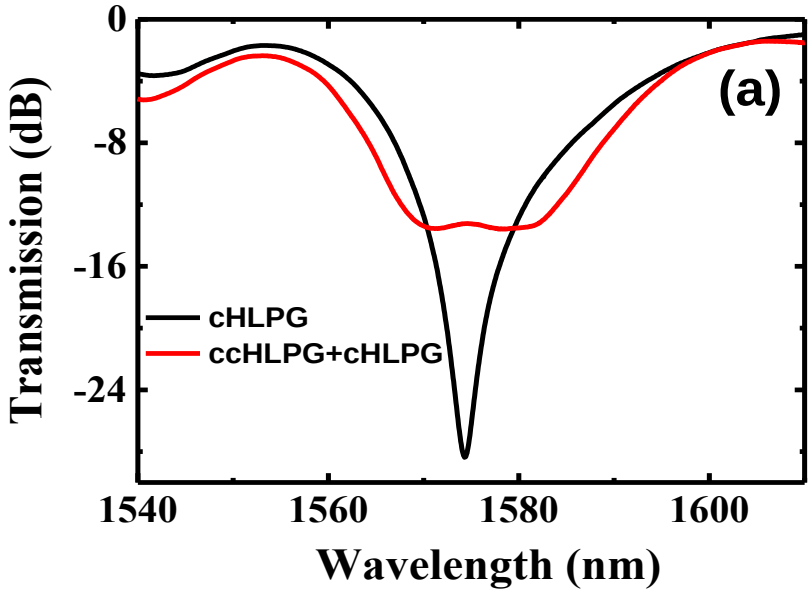

Fig. 7.2.1(a). Transmission spectrum of the cascaded HLPGs, where the solid black line shows the spectrum of the first grating cHLPG

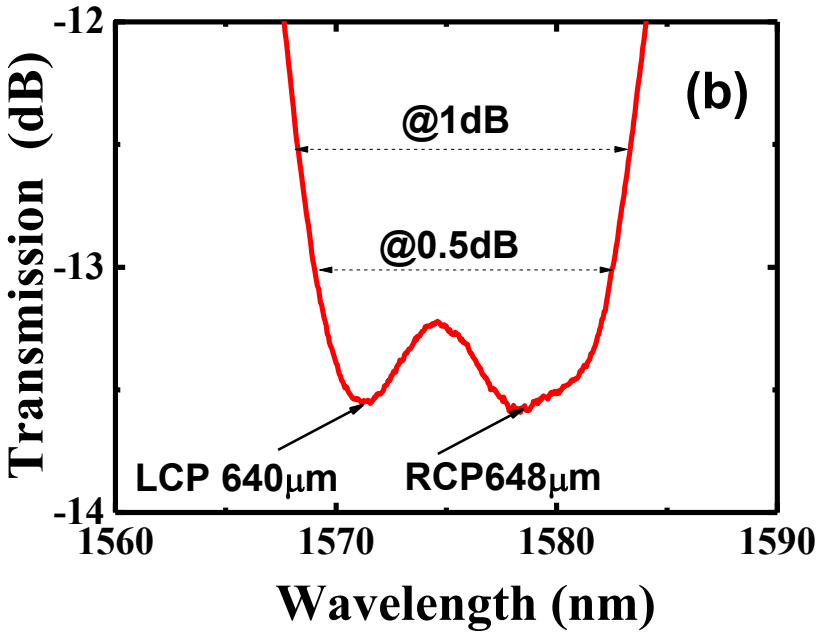

Fig. 7.2.1(b). a magnification part of the Fig. 7.2.1(a) near the center wavelength region

Then we measured the transmission spectrum of these two cascaded HLPGs, which was shown in Fig. 7.2.1(a) labeled by the red solid line. Frank speaking, the result obtained here is totally beyond our expectations, a fine flat-top filter with a rejection-band of ~15 nm@0.5dB and ~20 nm@1dB has been successfully obtained. Fig.7.2.1(b) shows a magnification part of the Fig. 7.2.1(a) at the central wavelength of 1574.50 nm region. It is obviously seen that there exist two small peaks (labeled with an arrow of LCP and RCP) in the flat-top band and central wavelength of the band almost lies in the same position as that of the cHLP (i. e, black line shown in Fig. 7.2.1(a)). To make further clear the mechanism of the resulted band-rejection filter, we also investigated the polarization dependence of the transmission spectrum by adding a fiber polarizer (Thorlabs: IPP1550SM-FC) and a fiber polarization controller (PC) right after the ASE source, the measuring results are shown in Fig. 7.2.2, where two particularly polarization status for the input light: a left circular polarization (LCP) and a right circular polarization (RCP) are particularly selected. However, due to the polarization scrambling effect most probably existed in the connecting fiber (SMF) between the PC and the two HLPGs, 100% of LCP and RCP light cannot be

obtained in our case, where a small portions of the light with a random-polarization (RP) status are inevitable. To compare Fig. 7.2.1(b) with the Fig. 7.2.2, it can be seen that the two peaks existed in the flat-top band (Fig. 7.2.1(b)) are strongly dependence on the polarization status of the incident light, which may be attributed to the two kinds of circular polarization light, respectively. Recently, it has been reported by G. Wong et al. that there exists newly-created circular-birefringence in a twisted photonic crystal fiber [22, 23]. In our case, due to the core-cladding eccentricity in the pristine fiber [5-6, 8], it is believed that the newly circular birefringence may also be generated, which would split the degenerated HE_{11} mode (with effective index of n_{eff}) into two de-degenerate modes: one is the right circular polarization (RCP) mode with effective index n_{eff}^{RCP} and the other is the left circular polarization (LCP) mode with effective index n_{eff}^{LCP}. Although the cladding mode LP_{12} may undoes the same de-degeneration procedure, the two cascaded HLPG will become cHLPG with 648μm and left polarization light and ccHLPG with 640μm and right polarization light. Therefore it is believed that the transmission spectrum shown in Fig. 7.2.1(b) can be regarded as the superposition one resulted from three individual gratings but without any interference.

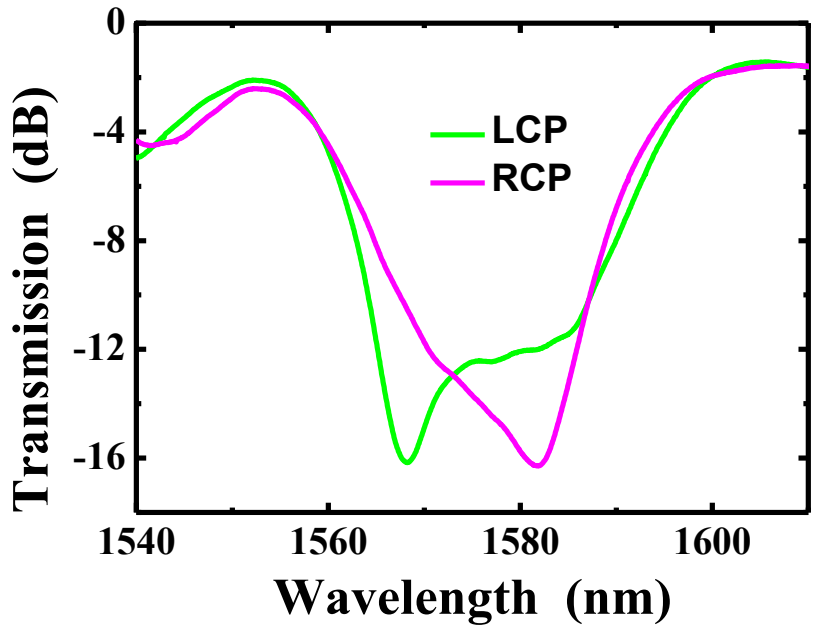

Fig. 7.2.2. Polarization properties for the transmission spectrum of the cascaded HLPGs

7.3 Numerical analysis for the flat-top band-rejection filter based on the successively cascaded helical LPGs

To verify the above proposal for principle of the resulted band-rejection filter, we had done some numerical simulations for the phase-shift LPGs using the transfer matrix method [24-26] under the conditions of different polarizations of the incident light. For convenience, we limit our calculations to a HLPG where there only exists a coupling between the core mode (LP_{01}) and the hybrid cladding mode LP_{12} within the wavelength region of 1500-1610 nm [7, 8]. More specifically, the parameters such as the radii of the core a_1 and cladding a_2, the refractive indexes of the core n_1 and cladding n_2, and the surrounding material n_3, are particularly chosen as: a_1=8.2, a_2=125 μm, n_1=1.4580, n_2=1.4536, and n_3=1.0. All the other parameters related to the HLPGs such as the grating period and grating length are the same as the ones used in our experiments. Because of if the two cascaded HLPGs have same rotation direction, the two cascaded gratings will form mutual interference like Fig 3.44. In this work, the two cascaded HLPGs have different rotation direction, so the two gratings will not form interference. Moreover, the red line in Fig. 7.3.1(a) shows the superposition spectrum of the other two individual gratings, and Fig. 7.3.1(b) shows superposition spectra of the LCP and NP, RCP and NP, respectively. It is seen that roughly the same as the experimental one, a flat-top band-rejection filter (Red solid line in Fig. 7.3.1(a)) has been obtained. Moreover, to compare the results shown in Fig. 7.2.2 and Fig. 7.3.1(b), it is obviously seen that the simulation results somehow agree with the experimental ones especially for the spectral envelopes, which qualitatively testify that the proposed flat-top band-rejection filter works well and the principle analysis proposed in this study may be reasonable. We think because of the structure of fabricated cascaded HLPGS or the reason for the other instruments can`t select LCP light and RCP light 100%, so the Fig. 7.3.1(b) more in line with our results.

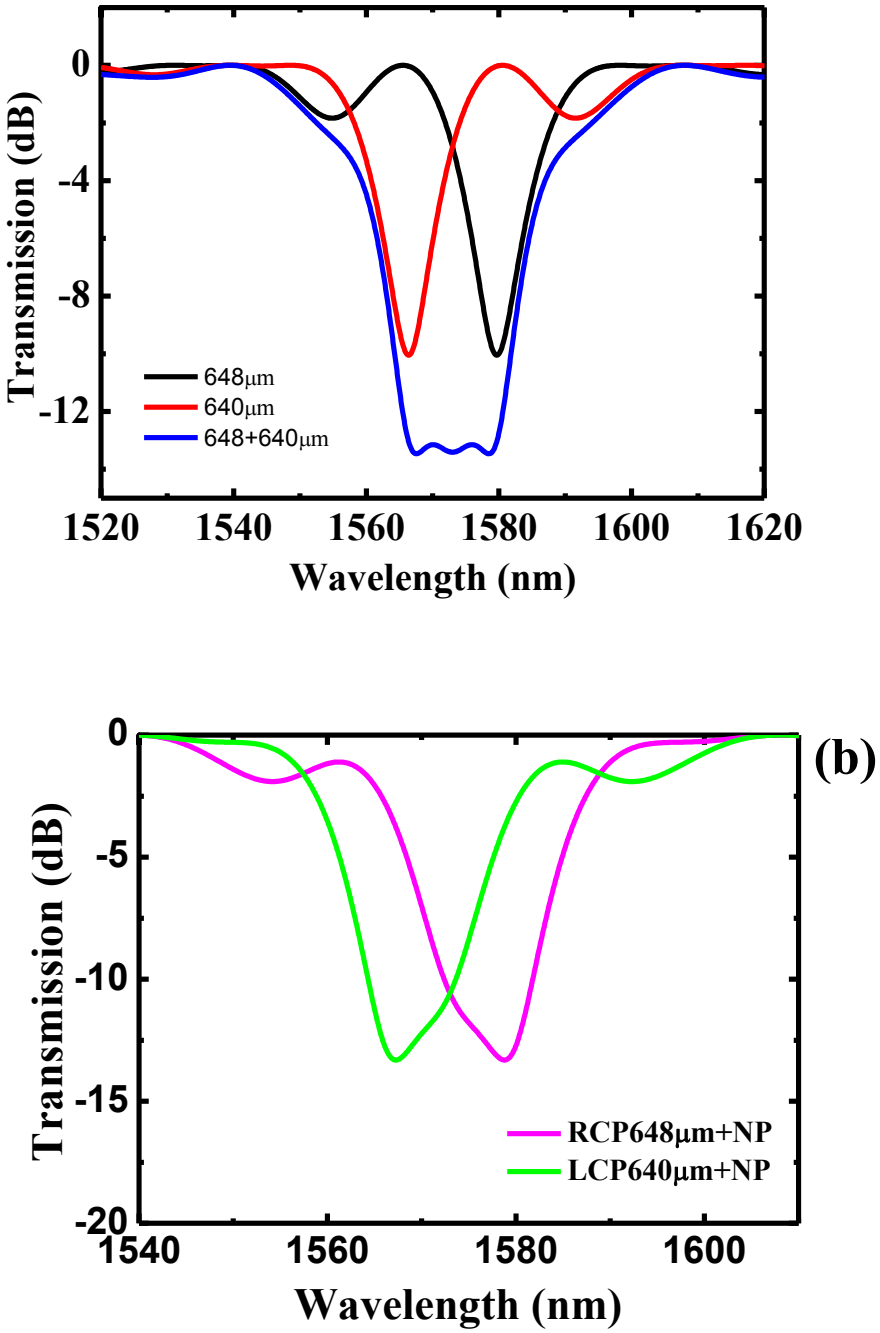

Fig. 7.3.1. Theoretical simulation for the transmission spectrum of the cascaded HLPGS, where the red line in Fig. 7.3.1(a) shows the superposition spectrum of the other two individual gratings, and Fig. 7.3.1(b) shows superposition spectra of the LCP and NP, RCP and NP, respectively.

7.4 Summary

A simple and robust method enabling to fabricate Helical LPG with a flat-top rejection-band has been proposed and demonstrated. Unlike most of the previous approaches, the proposed LPGs have a relative short length (less than 4.6 cm) and do not require a complex apodization in grating's amplitude, which makes this kind of HLPGs particularly suitable to be fabricated by using the robust CO_2 laser writing technique. As an example, a flat-top band-rejection filter with a bandwidth of ~13 nm@0.5dB and ~15 nm@1dB has been obtained, which is the broadest one reported to date, based on our knowledge, and may find further applications to the fields of fiber communication, fiber sensing, and all-optical information processing.

References

[1]. C. D. Pool, C. D. Townsend, and K. T. Nelson, "Helical-grating two-mode fiber spatial-mode coupler," J. Lightwave Technol. 9, 598–604 (1991).

[2]. V. I. Kopp, V. M. Churikov, J. Singer, N. Chao, D. Neugroschl, and A. Z. GenacK, "Chiral fiber gratings," Science 305, 74-75 (2004).

[3]. S. Oh, K. Lee, U. Paek, and Y. Chung, "Fabricatin of helical long-period fiber gratings by use of a CO_2 laser," Opt. Lett. 29, 1464-1466 (2004).

[4]. W. Shin, B. Yu, Y. Noh, Z. Lee, and D. Ko, "Bandwidth-tunable band-rejection filter based on helicoidal fiber grating pair grating of opposite helicitied," Opt. Lett. 32, 1214-1216 (2007).

[5]. Ivanov, "Fabrication of long-period fiber gratings by twisting a standard single-mode fiber," Opt. Lett. 30, 3290-3292 (2005).

[6]. G. Shvets, S. Trendafilov, V. I. Kopp, D. Neugroschl, and A. Z. Genack, "Polarization properties of chiral fiber gratings," J. Opt. A: Pure Appl. Opt. 11, 074007-1-10 (2009).

[7]. L. Xian, P. Wang, and H. Li, "Power-interrogated and simultaneous measurement of

temperature and torsion using paired helical long-period fiber gratings with opposite helicities," Opt. Express 22, 20260-20267 (2014).

[8]. Peng Wang and H. Li, "Helical long-period grating formed in a thinned fiber and its application to refractometric sensor," Applied Optics 55, in Press (2016).

[9]. C. N. Alexeyev, T. A. Fadeyeva, B. P. Lapin, and M. A. Yavorsky, "Generation and conversion of optical vortices in long-period twisted elliptical fibers," Appl. Opt. 51, C193-C197 (2012).

[10]. H. Xu and L. Yang, "Conversion of orbital angular momentum of light in chiral fiber gratings," Opt. Lett. 38, 1978-1980 (2013).

[11]. D. D. Davis, T. K. Gaylord, E. N. Glytsis, S. G. Kosinski, S. C. Mettler, and A. M. Vengsarkar, "Long-period fibre grating fabrication with focused CO_2 laser pulses," Electron. Lett. 34, 302-303 (1998).

[12]. Y. Rao, Y. Wang, Z. Ran, and T. Zhu, "Novel fiber-optic sensors based on long-period fiber gratings written by high-frequency CO_2 laser pulses," J. Lightwave Technol. 21, 1320-1327 (2003).

[13]. M. Sumetsky, Y. Dulashko, and A. Hale, "Fabrication and study of bent and coiled free silica nanowires: Self-coupling microloop optical interferometer," Opt. Express 12, 3521-3531 (2004).

[14]. A. Vengsarkar, P. Lemaire, J. Judkins, V. Bhatia, T. Erdogan, and J. Sipe, "Long-period fiber gratings as band-rejection filters," J. Lightwave Technol. 3, 58–65 (1996).

[15]. J. K. Brenne and J. Skaar, "Design of grating-assisted co-directional couplers with discrete inverse-scattering algorithms," J. Lightwave Technol. 21, 254–262 (2003).

[16]. J. Zhang, P. Shum, S. Li, N. Ngo, X. Cheng, and J. Ng, "Design and fabrication of flat-band long-period grating," IEEE Photon. Techn. Lett. 15, 1558–1560 (2003).

[17]. H. Kim, J. Bae, and J. Chun, "Synthesis of flat-top bandpass filters using two-band rejection long-period fiber gratings," IEEE Photon. Techn. Lett. 19, 1466–1468 (2007).

[18]. G. Chern and L. Wang, “Design of binary long-period fiber grating filters by the inverse-scattering method with genetic algorithm optimization,” J. Opt. Soc. Am. A. 19, 772-779 (2002).

[19]. H. Ke, K. S. Chiang, and J. Peng, “Analysis of phase-shifted long-period fiber gratings,” IEEE Photon. Techn. Lett. 10, 1596–1598 (1998).

[20]. Y. Liu, J. A. R. Williams, L. Zhang, and I. Bennion, “Phase shifted and cascaded long-period fiber gratings,” Opt. Commun. 164, 27–31 (1999).

[21]. L. R. Chen, “Design of flat-top bandpass filter based on symmetric multiple phase-shifted long-period fiber gratings,” Opt. Commun. 205, 271–276 (2002).

[22]. G. K. L. Wong, M. S. Kang, H. W. Lee, F. Biancalana, C. Conti, T. Weiss, P. St. J. Russell, “Excitation of orbital angular momentum resonances in helically twisted photonic crystal fiber,” Science 337, 446–449 (2012).

[23]. X. Xi, G. Wong, F. Biancalana, S. M. Barnet, M. J. Padgett, and P. St. J. Russell, “Optical activity in twisted solid-core photonic crystal fibers,” Phys. Rev. Lett. 110, 143903-1-5 (2013).

[24]. K. Hishiki and H. Li, “Phase-shift formed in a long period fiber grating and its application to the measurements of temperature and refractive-index,” Opt. Express 21, 11901-11912 (2013).

[25]. T. Erdogan, “Fiber Grating Spectra,” J. Lightwave Technol. 15, 1277-1294 (1997).

[26]. T. Erdogan, “Cladding-mode resonances in short- and long-period fiber gratings filters,” J. Opt. Soc. Am. A 14, 1760-1773 (1999).

8. Conclusions

This thesis is mainly concentrated on the study of helical long period fiber grating and its applications.

Firstly, we successfully achieved the LPG by using CO_2 laser irradiation method. Several kinds of phase-shifted LPGs are experimentally demonstrated by using the same method, where both the grating and the inserted phase-shift are obtained simultaneously in a single-mode fiber. As an application of this kind of gratings, a novel phase-shifted LPG-based sensor that allows for temperature- insensitive strain measurement has been proposed and successfully demonstrated. The measurement accuracy for the strain was estimated to be ±30 με within the range of 340-7600 με while the temperature is changed in the range of 20-140 °C.

Next, firstly we have been introduced a simple review on the developments of the HLPG to date. Secondly, an new kind of method to fabricate this kinds of gratings has been proposed and successfully demonstrated, which is based on the utilization of a CO_2 laser combined with a sapphire tube technique. Thirdly, a qualitative analyses on the forming mechanism of the proposed HLPG have been addressed. Finally, we make a qualitative analysis of the mechanism of forming HLPG. Finally, based on the hypothesis of the core-eccentricity mechanism, coupled-modes equations for the HLPG have also been discussed.

Referring to the applications of the HLPG, a new method enabling to fabricate HLPGs in a thinned fiber with a diameter smaller than several tens of micrometers has been proposed and experimentally demonstrated, where a sapphire tube is particularly utilized in place of the focal lens. As an application of this kind of HLPGs, a novel fiber refractometric sensor that allows for temperature-insensitive measurement of the refractive index has been proposed and successfully demonstrated. It is expected that this kind of HLPGs may find potential applications to high-sensitive fiber sensors, mode-converter and orbital angular momentum beams in optical communications.

Finally, we have proposed and demonstrated the applications of HLPG to optical communication filed. For example, a simple and robust method enabling to fabricate Helical LPG with a flat-top rejection-band has been proposed and demonstrated. Unlike most of the previous approaches, the proposed LPGs have a relative short length (less than 4.6 cm) and do not require a complex apodization in grating's amplitude, which makes this kind of HLPGs particularly suitable to be fabricated by using the robust CO_2 laser writing technique. As an example, a flat-top band-rejection filter with a bandwidth of ~13 nm@0.5dB and ~15 nm@1dB has been obtained, which is the broadest one reported to date, and may find further applications to the fields of fiber communication, fiber sensing, and all-optical information processing.

Publications

Journal papers

1. Gen. Inoue, **Peng Wang**, and Hongpu Li “Flat-top band-rejection filter based on two successively-cascaded helical fiber gratings,” Optical Express Vol. 24, No. 5, Mar 7, 2016.

2. **Peng Wang** and Hongpu Li “Helical long-period grating formed in a thinned fiber and its application to a refractometric sensor,” Applied Optics, Vol. 55, No. 6, February 20, 2016.

3. **Peng Wang**, Lunlun Xian, and Hongpu Li “Fabrication of a phase-shifted long-period fiber grating and its application to strain measurement，”IEEE Photonics Technology Letters, Vol. 27, No. 5, March 1, 2015.

4. Lunlun Xian, **Peng Wang**, and Hongpu Li “Power-interrogated and simultaneous measurement of temperature and torsion using paired helical long-period fiber gratings with opposite helicities,” Optical Express Vol. 22, No. 17, Aug 25, 2014.

5. Lunlun Xian, **Peng Wang**, Kazuhiko Ogusu, and Hongpu Li “Cladding mode coupling in a wide-band fiber Bragg grating and its application to a power-interrogated temperature sensor,” IEEE Photonics Technology Letters, Vol. 25, No. 3 231-233 2013.

Conferences papers

1) Optoelectronics and communications conference / International conference on photonics in switching（新潟）2016 年 7 月 7 日

Flat-top band-rejection filter based on helical long-period fiber grating (ThC3-1**)**

Peng Wang・Gen Inoue・Hongpu Li（Shizuoka Univ.）

2) 電子情報通信学会（福岡）2016 年 3 月 18 日

Flat-top band-rejection filter based on helical long-period fiber grating (C-3-62**)**

Peng Wang・Gen Inoue・Hongpu Li（Shizuoka Univ.）

3) 電子情報通信学会（仙台）2015 年 9 月 10 日

Helical long-period grating formed in a thinned fiber and its application to temperature-insensitive refractometric sensor (C-3-40**)**

Peng Wang・Hongpu Li（Shizuoka Univ.）

4) 電子情報通信学会（草津）2015 年 3 月 13 日

Fabrication of a long-length microfiber by using a CO2 laser (C-3-57**)**

Peng Wang・Hongpu Li（Shizuoka Univ.）

5) 電子情報通信学会 (徳島) 2014 年 9 月 23 日

Fabrication of a phase-shifted long-period fiber grating and its thermal and strain characteristics (C-3-17**)**

Peng Wang・Hongpu Li（Shizuoka Univ.）

6) 電子情報通信学会（新潟）2014 年 3 月 18 日

長周期ファイバグレーティングを用いたパワーインタロゲーション温度センサーの実現 (C-3-10)

日紫喜 圭介・王 **鵬・細越 賢人・李 洪譜**（Shizuoka Univ.）

7) **電子情報通信学会（福岡）2013 年 9 月 18 日**

Microfiber interferometer fabricated by using CO_2 laser and its application to a temperature-insensitive refractometric sensor (C-3-66)

Peng Wang・Keisuke Hishiki・Lunlun Xian・Hongpu Li（Shizuoka Univ.）